Journal of Asian Earth Sciences 44 (2012) 117–135

Contents lists available at ScienceDirect

Journal of Asian Earth Sciences

journal homepage: www.elsevier.com/locate/jseaes

# Magnetostratigraphy of the Neogene Siwalik Group in the far eastern Himalaya: Kameng section, Arunachal Pradesh, India

François Chirouze [a,*], Guillaume Dupont-Nivet [b,c], Pascale Huyghe [a], Peter van der Beek [a], Tapan Chakraborti [d], Matthias Bernet [a], Véronique Erens [b]

[a] Institut des Sciences de la Terre, Université Joseph Fourier, 1381 Rue de la piscine, BP 53, 38041 Grenoble Cedex, France
[b] Paleomagnetic Laboratory Fort Hoofddijk, Faculty of Geosciences, Utrecht University, Budapestlaan 17, 3584 CD Utrecht, The Netherlands
[c] Geosciences Rennes UMR-CNRS 6118, 263 Avenue du General Leclerc, Campus de Beaulieu Bat.15, CS 74205, 35042 Rennes Cedex, France
[d] Geological Studies Unit, Indian Statistical Institute, 203 B.T. Road, Kolkata 700 108, India

ARTICLE INFO

*Article history:*
Available online 12 June 2011

*Keywords:*
Foreland basin
Far eastern Himalaya
Magnetostratigraphy
Siwaliks
Greigite
Tectonic rotation

ABSTRACT

The Siwalik Group was deposited from the Mid-Miocene to the Pliocene in the foreland of the Himalaya and records the unroofing history of the mountain belt. In this study we provide the first magnetostratigraphic data for the eastern Himalayan foreland basin. We analyzed two sections of the lower to upper Siwalik Group along the Kameng River in Arunachal Pradesh, India. Magnetostratigraphic data were acquired from 395 sites within a 5.8 km-thick molassic series. Thermal demagnetization and magnetic rock-property analyses indicate a relatively low temperature (150–340 °C) Characteristic Remanent Magnetization (ChRM) yielding reliable primary directions carried by iron sulfides such as greigite. The results show local counter-clockwise rotation of the thrust sheets, which is consistent with partitioning of arc-normal and left-lateral strain along the Himalaya. Nineteen polarity zones have been identified in the two sections. Detrital fission-track data from the top and bottom of the sections are used to constrain correlations with the geomagnetic polarity time scale (GPTS) from chron C5Ar.1n to chron C2An.2n. From these results, we propose that the Siwalik Formation in Arunachal Pradesh was deposited between 13 and 2.5 Ma. The transition between the lower and middle Siwaliks is dated at about 10.5 Ma and the middle to upper Siwaliks transition is dated at 2.6 Ma. These results, coupled with sedimentological observations, suggest that the eastern Himalayan chrono-stratigraphic record is nearly synchronous with that analyzed in other parts of the Neogene Himalayan foreland basin. Nevertheless, some differences in the evolution of the sedimentation rate and in the thickness of the middle Siwaliks suggest that Indian plate flexure in the East is different from that observed in other parts of the Indian foreland basin, and could be affected by the presence of the Shillong Plateau to the south.



## 1. Introduction

Foreland basins act as receptacles for synorogenic sediments and store material eroded off a convergent mountain belt. Their infill records tectonic, climatic and erosional processes that govern the development of the mountain belt and the foreland basin. Consequently, studying the infill of foreland basins provides clues for the reconstruction of the tectonic growth of the orogen and its interaction with global or regional climate (e.g. DeCelles and Giles, 1996). Tectonic, erosional and climatic events affecting the Himalaya are recorded in the Neogene Siwalik foreland basin deposits (e.g. DeCelles et al., 1998, 2000; Huyghe et al., 2001, 2005; Najman et al., 2005). These sediments are dated using magnetostratigraphy to provide a temporal framework for analyses of the sedimentary record in terms of provenance, structural geology, thermochronology and paleoclimate. Magnetostratigraphic dating has yielded ages of the central and western Himalayan foreland deposits guided by biostratigraphy and, mostly in the western foreland, rare radiochronologic constraints (e.g. Johnson et al., 1982a,b, 1985; Gautam and Rösler, 1999; Ojha et al., 2000, 2009). However, very few studies address the eastern part of the Himalayan foreland basin (e.g. Yin et al., 2006, 2010; Cina et al., 2009), even though understanding the evolution of this eastern part is essential for reconstructing the regional migration of Himalayan deformation. In addition, the eastern Himalayan foreland potentially contains a record of the exhumation of the eastern syntaxis (Singh and France-Lanord, 2002; Stewart et al., 2008), Shillong Plateau uplift (Biswas et al., 2007; Clark and Bilham, 2008) and the related evolution of the Brahmaputra drainage network. Therefore, accurate dating of the sediments in the eastern part of the Siwalik foreland basin using magnetostratigraphy is a crucial initial step for further

* Corresponding author.
*E-mail address:* frchirouze@gmail.com (F. Chirouze).

1367-9120/$ - see front matter © 2011 Elsevier Ltd. All rights reserved.
doi:10.1016/j.jseaes.2011.05.016

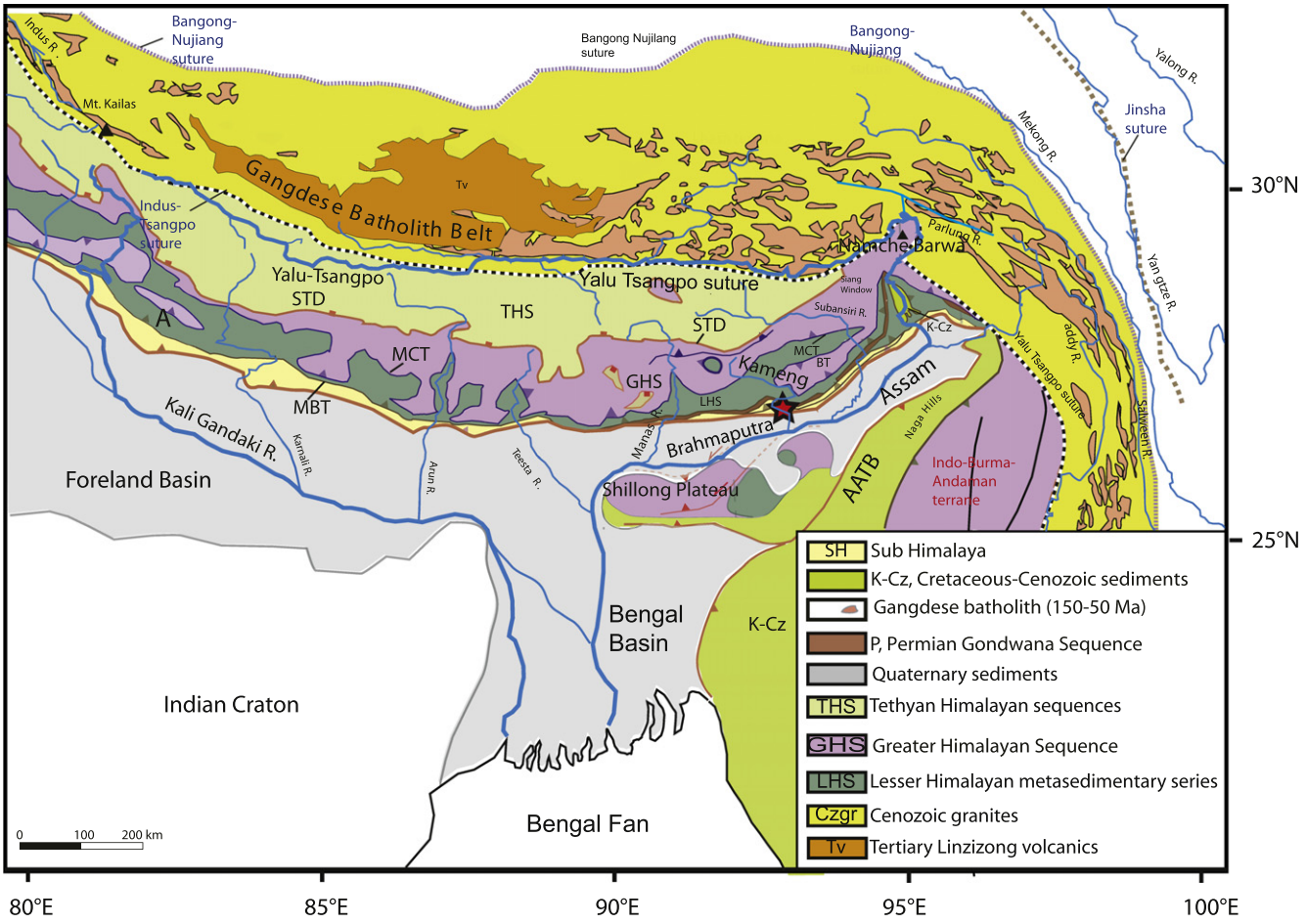


**Fig. 1.** Regional tectonic map showing simplified geology and locations of major rivers (after Yin et al. (2006, 2010) and Guillot and Charlet (2007)). Red star indicates location of Kameng section. Tectonic structures: Main Frontal Thrust (MFT), Main Boundary Thrust (MBT), Main Central Thrust (MCT), South Tibetan detachment (STD), and Assam-Arakan Thrust Belt (AATB). (For interpretation of the references to color in this figure legend, the reader is referred to the web version of this article.)

investigations permitting to constrain exhumation and climate of this part of the mountain chain. The purpose of this paper is to report the first magnetostratigraphic results from the Siwalik Group in the Eastern Himalaya. We have performed a magnetostratigraphic study along the Kameng River section in the far eastern district of Arunachal Pradesh, India (Figs. 1 and 2), where a thick series of Siwalik sediments is well exposed and accessible. Due to the lack of biostratigraphic and radiometric age constraints in this area, we refer here to detrital thermochronologic results of Chirouze (2011) to provide independent age control.

## 2. Geological setting

### 2.1. Himalayan geology

Collision between the Indian and Asian plates began in the Early Eocene (e.g., Yin and Harrison, 2000; Zhu et al., 2005; Dupont-Nivet et al., 2010), causing intense crustal shortening and imbrication of southward-displaced thrust sheets and resulting in the formation of the Himalayan mountain belt and Tibetan Plateau (e.g. Hodges, 2000; Yin and Harrison, 2000). The Himalaya is generally subdivided into four major lithotectonic units, which are from north to south: the Tethyan Himalayan zone (TH); the Higher or Greater Himalayan zone (HH); the Lesser Himalayan zone (LH); and the Sub-Himalayan zone (SH) (Fig. 1; e.g. Gansser, 1964; Valdiya, 1980; Upreti, 1999).

These lithotectonic units are bounded by late Cenozoic north-dipping fault systems branching off the Main Himalayan Thrust (MHT). They include, from north to south: the South Tibetan Detachment (STD); the Main Central Thrust (MCT); the Main Boundary Thrust (MBT); and the Main Frontal Thrust (MFT) (Fig. 1). The latter thrust puts Siwalik strata over the Indus-, Ganges- and Brahmaputra-alluvial plains, respectively in front of the western, central and eastern Himalayan belt, the latter being the focus of this study. The MFT locally cuts Siwalik strata at the surface but is often blind.

### 2.2. Stratigraphy of the tertiary basins

The SH rocks consist of clastic synorogenic sediments filling the Neogene Himalayan foreland basin from Assam (India) to Pakistan. These sediments are folded and thrust because of ongoing shortening and forward thrust propagation during Cenozoic time. Therefore, they are incorporated in the outer part of the orogenic belt, forming the Sub-Himalayan range (elevation from 200 to 1500 m). In the north-western (Pakistan or Himachal Pradesh, India) and central (Nepal) parts of the foreland basin, the SH sediments are composed of fluvial material (Tandon, 1976; Willis, 1993; Nakayama and Ulak, 1999), which was deposited from Late Miocene to Late Pliocene times (Najman, 2006; DeCelles et al., 1998) and is generally referred to as the Siwalik Group. In Nepal and western India, the Siwalik Group is about 5000 m thick (Ojha et al., 2009; Gautam and Fujiwara, 2000; White et al., 2001). It

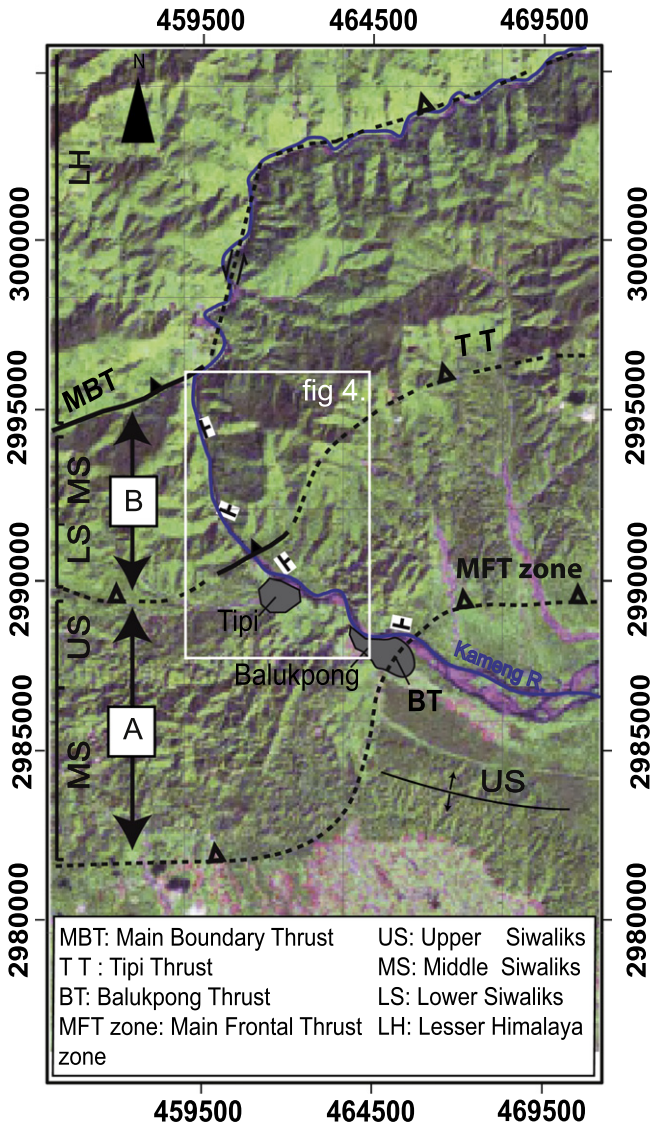


**Fig. 2.** Local tectonic map of the Kameng area showing tectonic structures. The positions of the sampled sections A and B are indicated in boxes. Grid reference is UTM.

comprises a succession of grey mudstone, siltstone, and fine to coarse-grained sandstone. Individual sand bodies mostly fine upwards, but form a coarsening and thickening upward succession on the scale of the entire Siwalik Group. In Nepal, sediment accumulation rates range from 0.28 to 0.56 mm/year, generally increasing through time (Ojha et al., 2009).

The Siwalik Group is classically subdivided into three informal units (DeCelles et al., 1998; Nakayama and Ulak, 1999). The lower Siwaliks (LS) consist of an alternation of fine- to medium-grained sandstones and mudstones forming sedimentary cycles with a thickness of a few meters. They were deposited by meandering river systems. The middle Siwaliks (MS) are medium to coarse grained, grey, mica-rich sandstones. Individual beds are commonly several tens of meters thick. Their deposition is attributed to a braided river system. The upper Siwaliks (US) consist of pebble and cobble conglomerates, with beds commonly tens of meters in thickness intercalated with sandstone and clay layers. They formed as alluvial fan deposits near the mountain front.

The eastern foreland basin is surrounded by the Assam–Arakan thrust belt to the east and the Shillong Plateau to the south, and overlies the NE termination of the pre-existing Bengal basin (Alam et al., 2003). Provenance analysis in the NW shelf of the Bengal basin suggests that significant input of Himalayan-derived material began during the Early Miocene in the Barail deltaic Formation (Najman et al., 2008). In the NE (Assam basin), lower Miocene fluvial sandstone (Tipam Formation) contains heavy mineral suites compatible with input from the rising Himalaya (Bhandari et al., 1973). The transition from deltaic to fluvial environments is estimated to have occurred between the Middle and the Late Miocene (Kent and Dasgupta, 2004). Nonetheless, in contrast to the well-known continental fluvial origin of the Siwalik rocks of the western and central Himalaya, the Neogene environment in Arunachal Pradesh displays a strong influence of brackish water or a near coastal setting, as evidenced by paleobotanical studies (Singh and Prakash, 1980; Singh and Tripathi, 1990; Mehrotra et al., 1999). Some workers have suggested that the Siwalik foreland basin of Arunachal Pradesh was not connected to the Siwalik basin of the western Himalaya (Rao, 1983; Sinha et al., 1982).

## 3. The Kameng River section

### 3.1. Sedimentology of Neogene strata along the Kameng River section

A host of palynomorphs, leaf impressions and fossil wood species have been reported from the Siwaliks of Arunachal Pradesh. Although these studies lack stratigraphic control, limiting their usability, they do indicate a general Miocene age of deposition (Singh, 1977; Dutta, 1980). In the following, we use the local litho-stratigraphic classification, which subdivides the Neogene succession into the Dafla, Subansiri and Kimin Formation from base to top (Karunakaran and Rao, 1976; Kumar, 1997). Following Yin (2006), these three formations may be broadly correlated to the lower, middle and upper Siwaliks of other parts of the Himalayan foreland basin. Their general descriptions are as follows:

The Dafla Formation (LS) shows fine- to medium-grained sandstone alternating with thinner beds of drab-colored silt-shale layers. Indurate sandstone beds are 2–10 m thick, usually show a flat base strewn with mudclasts and comprise dominantly low-angle to plane parallel stratification. The sandstone beds are overlain by silt–clay units with sharp contacts. The silt–clay beds contain abundant wave ripples, burrow marks and leaf impressions. Thin grey paleosols are locally developed, with 2–8 cm long probable root traces (Fig. 3A and B). The deposition of this formation may be attributed to low-gradient sinuous channels in a lacustrine or marine deltaic setting (Tye and Coleman, 1989; Perez-Arlucea and Smith, 1999; Griffing et al., 2000).

The Subansiri Formation (MS) comprises thick beds of friable "salt-and-pepper" sandstone with grainsize ranging from pebbly, very coarse to medium sand. In the lower part of this formation, beds are a few meters thick and are intercalated with well-developed organic-rich grey mudstone or siltstone layers. In the upper part of the Subansiri Formation, beds are up to 10 m thick and show large-scale cross-stratification and abundant calcareous nodules of 0.1–1 m in diameter. Many of the sandstone beds show pebbly layers near their base. Several tens of meters thick amalgamated sandstone bodies form cliffs in the landscape (Fig. 3C). The deposition of this formation may be attributed to a braided river system.

The Kimin Formation (US) is characterized by pebble-boulder conglomerates interlayered with sandstone and shale. Bands of pebble-cobble conglomerates are 0.3–7 m thick and alternate with yellow–orange coarse-grained to gritty sandstone and 0.5–5 m thick red to variegated clay (Fig. 3D and E). Carbonized fossil wood fragments up to 1 m long are common. The Kimin sediments were possibly formed as alluvial fan deposits relatively close to the mountain front.

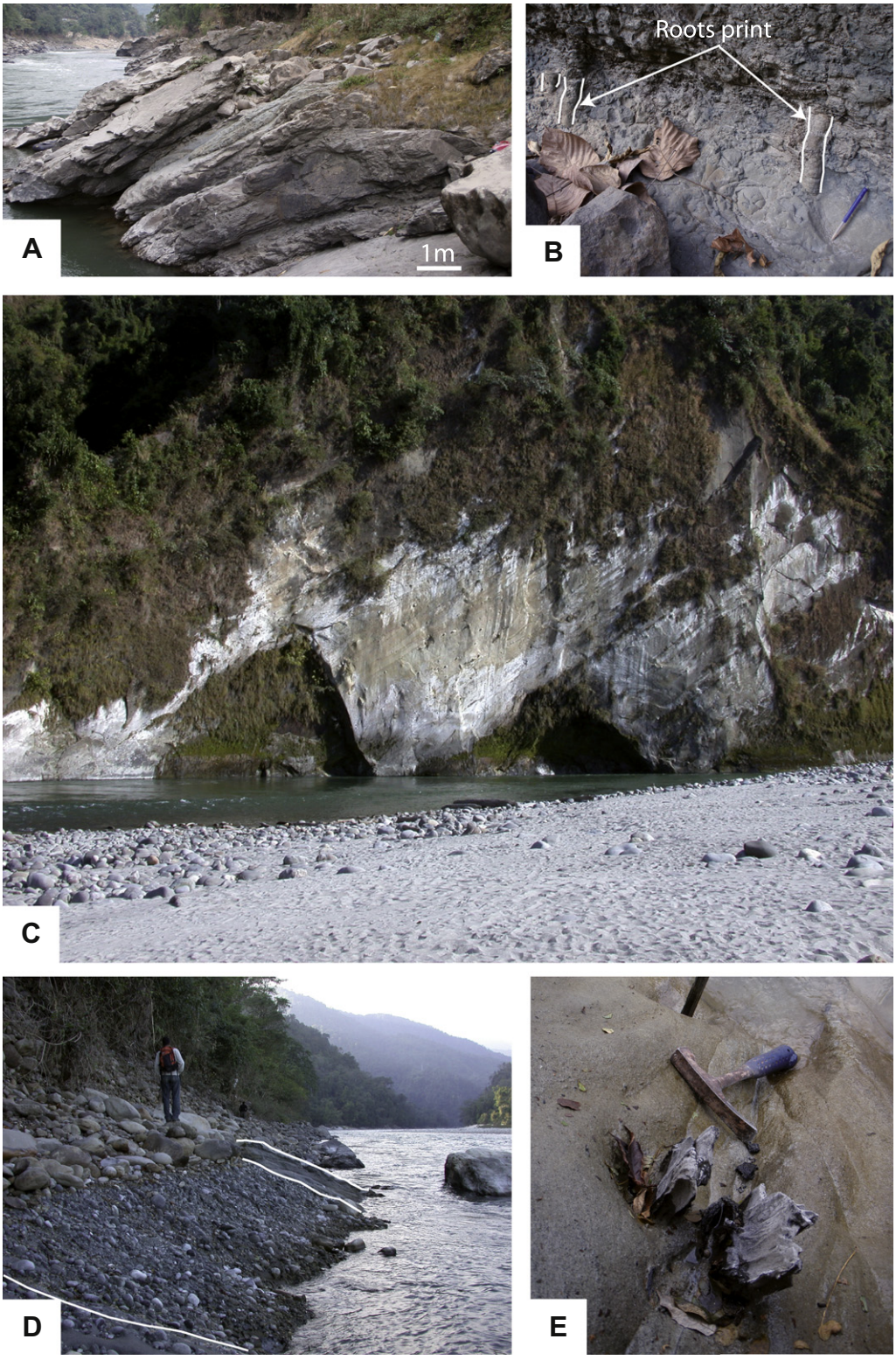


**Fig. 3.** Typical sedimentary facies recognized along the Kameng section. (A) Typical image of Dafla Formation sandstone–mudstone alternations. (B) Paleosol layers with roots prints in Dafla Formation. (C) Typical outcrop of Subansiri Formation coarse sandstone. Thick beds are composed of numerous amalgamated channels. (D) Alternation of boulder and sandstone layers in the Kimin Formation. (E) Wood fragment in the Kimin Formation.

### *3.2. Structural setting of the Kameng section*

Three main tectono-geomorphic features are observed from south to north in the studied area of the Kameng River (Fig. 2). The MFT is locally materialized by a zone of discontinuous folds, thrusts and strike slip faults (Yin et al., 2010), which separate the Brahmaputra alluvial plain from the Neogene succession in outermost foothills of the Himalayan belt (Singh and Chowdhary, 1990; Kumar, 1997). One portion of this zone, the Balukpong thrust, juxtaposes the Subansiri Formation over Quaternary sand and

gravel deposits and locally over the Kimin Formation (Yin et al., 2010). Close to the town of Balukpong, the E-W trending MFT zone locally turns to a NNE-SSW direction. The Tipi Thrust (Singh and Chowdhary, 1990; Acharyya, 1994) juxtaposes the Dafla Formation over the upper Kimin Formation and underlies the base of a second foothill range. This range displays a marked NE–SW virgation close to the village of Tipi (Fig. 2). The MBT constitutes the northern limit of the Neogene deposits and separates the Dafla Formation from the LH series. The base of the LH series directly above the MBT is composed of a north-dipping succession comprising Permian coal-bearing strata as well as augengneiss interlayered with phyllite, quartzite, metavolcanics and carbonate rocks, known as the Bomdila Group (Yin et al., 2006).

## 4. Sampling and laboratory methods

To provide constraints for the correlation of our paleomagnetic results with the geomagnetic polarity time scale (GPTS) in the absence of independent dating from biostratigraphy or volcanic ash layers, our magnetostratigaphic study is coupled with detrital fission-track analysis. The upper- and lower-most parts of the section will thus be assigned a maximum depositional age based on available fission-track cooling ages of detrital apatite and zircon from the sampled section (Chirouze, 2011).

### 4.1. Sampling methods and strategy

We sampled two distinct sections, in the footwall and hanging wall of the Tipi Thrust (respectively A and B in Fig. 2). Section A is located below the Tipi Thrust and thus comprises sediments of the lower part of the Kimin Formation and the Subansiri Formation. It is about 3700 m thick, but only the lower 2500 m of the section were sufficiently well exposed for continuous paleomagnetic sampling. Section B is located above the Tipi Thrust, comprises older sediments of the lower part of the Subansiri Formation (MS) and the upper Dafla Formation (LS) and is about 2400 m thick with relatively continuous exposure. Where possible, we limited the spacing of our paleomagnetic sites to 8 m (Fig. 4). Most of the exposures were fresh river outcrops but we could not avoid several gaps, sometimes exceeding 100 meters in the sampling scheme, especially in section A, due to lack of outcrop, unfavorable lithologies of limited access to the river banks. Two or three 2.5 cm diameter cylindrical rock cores were collected from each paleomagnetic site, targeting finer lithologies or mudstone layers, using an electric drill powered by a portable generator and mounted with a diamond-coated drill bit cooled with water. Cores were oriented with a custom device integrating a clinometer and a magnetic compass. Insignificant local declination (<0.5°) was neglected. As fine-grained beds were rare in the Subansiri Formation, coarser lithologies (medium to coarse sands) were also sampled in section A, as well as preserved early diagenetic nodules within otherwise heavily weathered sandstone banks. In total, the number of collected paleomagnetic samples amounts to 154 for the younger section A and 241 for the older section B. Bedding attitudes were measured at regular intervals and averaged for portions of the sections with similar attitudes for tilt corrections. Measured plunging of local and regional fold axes were not significant and not consistent throughout the sampled sections.

Medium-coarse sandstones were sampled for detrital apatite (AFT) and zircon fission-track (ZFT) analysis at strategic levels (Fig. 4; Chirouze, 2011). Taking into account the thickness of both sections A and B, an AFT sample was collected close to the top of the footwall section to avoid possible resetting of AFT ages linked to tectonic burial in addition to depositional burial in the basin. In the hanging-wall section B, we collected a sample for ZFT analysis close to the bottom of the section (Dafla Formation) in order to obtain an upper limit for the depositional age of the Kameng River section.

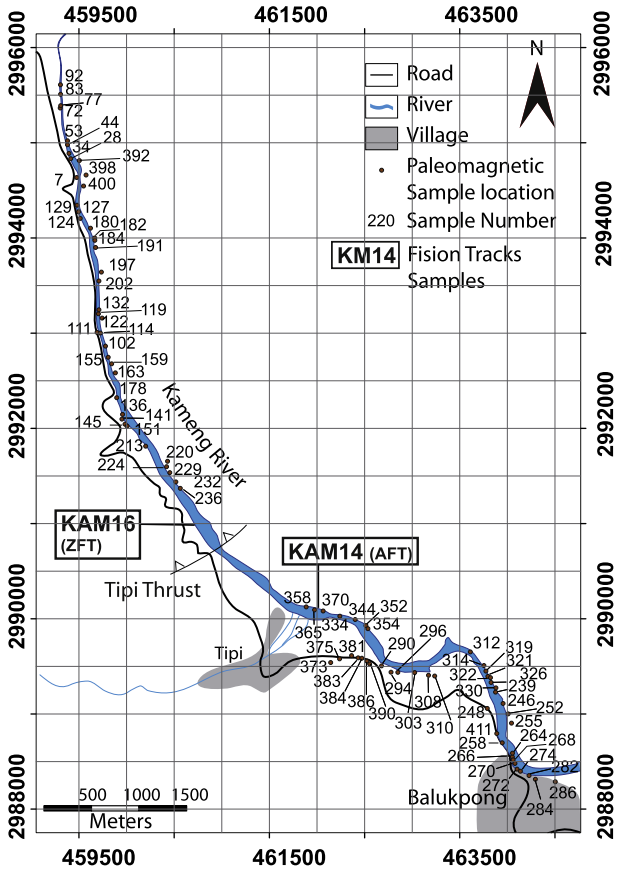


**Fig. 4.** Sample locations along the Kameng section. For clarity, only samples with GPS points used to calculate section thickness are presented. Grid reference is UTM.

### 4.2. Paleomagnetic analysis

Remanent magnetizations of samples were measured on a 2G Enterprises DC SQUID cryogenic magnetometer at the Utrecht University paleomagnetic laboratory. A first selection of pilot samples distributed every 40 m throughout the sampled stratigraphy was stepwise thermally demagnetized in a shielded oven in small steps from 20 °C to 600 °C in order to (1) determine characteristic demagnetization behavior, (2) establish the most efficient demagnetization temperature steps, (3) determine which lithology provides the best signal, and (4) localize stratigraphic intervals with potential paleomagnetic reversals. These results guided further processing of the following selections of samples, from key parts of the section, at higher stratigraphic resolution. Whenever the result from a single sample at a sampling level was ambiguous, a second or a third sample was processed and the best result was chosen to represent that sampling level.

Natural Remanent Magnetization (NRM) intensities are generally low throughout the section (average of 800 μA/m) suggesting small variations in magnetic mineralogy and the absence (or presence in only trace amounts) of strongly magnetic iron oxides such as magnetite. Four main Characteristic Remanent Magnetization (ChRM) components stand out on vector end-point diagrams and stereographic projections of the processed samples (Fig. 5): (1) a very low temperature component with normal polarity direction

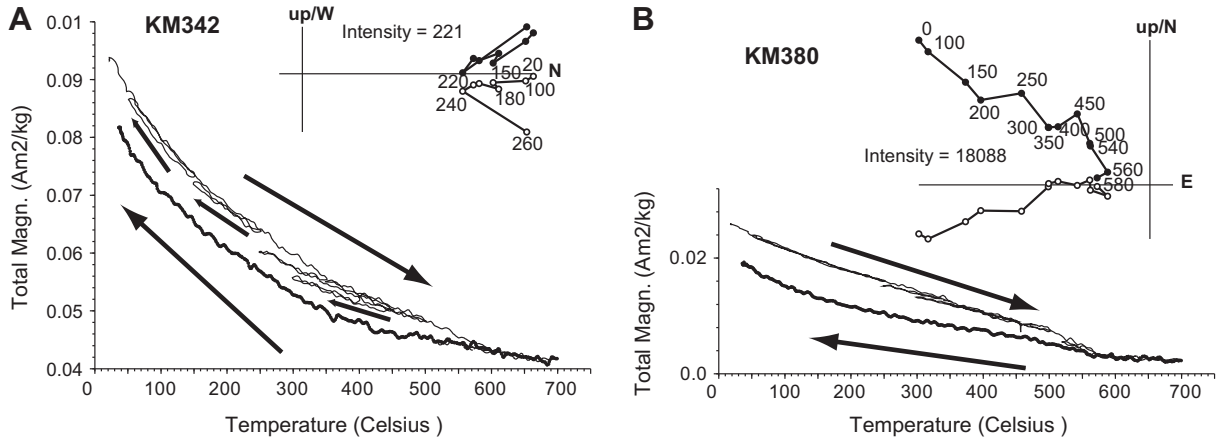


**Fig. 5.** Demagnetization diagrams (top) and rock magnetic experiment (bottom) showing typical behavior (see text for discussion). In demagnetization diagrams, full symbols are projections on the horizontal plane and open symbols on the vertical plane. The number next to the symbol indicates temperature of demagnetization step in °C. The starting intensity is given in $10^{-3}$ A/m. Bottom diagrams are results from horizontal translation type Curie balance of Utrecht University (Mullender et al., 1993). Runs during different heating and cooling cycles are shown. Behavior (A) of most samples from the Kameng section contrasts with behavior (B) of rare samples carrying a relatively high-temperature stable component.

demagnetized from 20 °C to 150 °C; (2) a low temperature component (LTC) from 150 °C to 240 °C; (3) a medium-temperature component (MTC) with normal or reversed polarity directions is typically demagnetized from 150 °C to 340 °C; and (4) a high-temperature component (HTC) with usually unstable directions and increasing magnetic intensity from ~340 °C to 600 °C.

This characteristic signal is associated with the production of a ferromagnetic phase during heating as confirmed in further rock-magnetic experiments (see below). In rare cases, the HTC component showed a steady decrease until 600 °C. To circumvent mineral transformations during heating, some pilot samples were also processed with a combination of thermal demagnetization up to 300 °C followed by alternating field (AF) demagnetization with a coupled 2G AF degausser at incremental steps up to 90 mT. Unfortunately, these experiments gave mixed results with erratic demagnetization paths (possibly related to gyroremanence) that were generally less effective in separating the ChRM components. Thus, only thermal demagnetization was applied to the rest of the samples with a careful set of small thermal demagnetization steps at low temperature (50 °C steps up to 150 °C and 30 °C steps from 150 °C to usually 330°-360 °C), after which sample intensities started to increase due to mineral transformations.

Rock-magnetic experiments were performed to assess the magnetic mineralogy and to better constrain the reliability of the ChRM. To test potential artifacts due to mineral transformation during stepwise heating, we subjected characteristic samples to high-field thermomagnetic runs in air using the modified horizontal translation type Curie balance of the University of Utrecht (Mullender et al., 1993) with a sensitivity of approximately $5 \times 10^{-9}$ Am$^2$. Runs during different heating and cooling cycles were performed at a rate of 10 °C min$^{-1}$ (Fig. 5). As expected, these experiments show the destruction of a mineral phase up to 300–350 °C for most samples (those with increasing intensities in demagnetization of the HTC), sometimes followed by increasing moments due to the production of a ferromagnetic mineral. The phase created is then destroyed at 580–600 °C, suggesting it is a mineral such as magnetite. In contrast, for the rare samples that showed a steady decreasing HTC upon thermal demagnetization, decreasing or reversible moments were observed at high temperatures (580–600 °C), suggesting the presence of original iron oxides such as magnetite in those samples. We interpret the thermomagnetic results, along with the thermal demagnetization behavior (magnetite production in the HTC) and typically low values of LTC and MTC to suggest the predominance of iron sulfides in most samples (e.g. Dunlop and Özdemir, 1997; Vasiliev et al., 2008). This intepretation is substantiated by recent reports of similar magnetic properties from greigite that has been shown to carry a primary remanence in successful magnetostratigraphic analysis of the Miocene Carpathian foredeep basin deposits from a brackish fluvio-deltaic environment (Vasiliev et al., 2004, 2005, 2008). To estimate whether the MTC carries a primary magnetization, the stability of ChRM directions was analyzed.

ChRM directions were calculated using a minimum of four consecutive steps of the MTC (150 °C to ~340 °C) decreasing towards the origin. Line fits were not anchored to the origin except for some demagnetization paths showing steady a direction but no significant decrease in intensity upon demagnetization of the MTC (e.g., KM22; Fig. 6a). Line fits with maximum angular deviation (MAD) above 30° were systematically rejected. ChRM directions are listed in the tables of the data repository (Appendix A, Tables A1 and A2). Because of occasional occurrences of a normal overprint of the LTC, sometimes extending to relatively high demagnetization temperatures (250 °C), a careful selection of ChRM directions (especially of normal directions) was performed by grouping them in three quality groups as follows (Fig. 6): For 78 ChRM directions (quality-1), normal or reversed polarities were clearly identified on the MTC by stable and linear demagnetization paths (MAD typically below 15°) that were well separated from the LTC. For 132 ChRM directions (quality-2), normal or reversed polarities are clearly indicated but the directions are less reliable, mainly because of directional scatter and/or partial LTC overlap on MTC. Great-circle analysis (McFadden and McElhinny, 1988) was applied for some of these samples, when the contribution of the normal direction LTC overlapped on a reversed polarity direction carried by only a few points of the MTC. For this procedure the mean of the quality-1 directions was used as set point. In general, the distinction of the MTC from the normal overprint was aided by the fact that the MTC directions have been affected by a significant counter-clockwise tectonic rotation (see below). Still, a significant proportion of the processed samples did not yield any interpretable results. For 81 unreliable ChRM directions (quality-3), the polarity determinations remain ambiguous due to the weakness of the signal and/or overlapping demagnetization with the normal-polarity LTC; these samples were thus rejected from further analysis. In addition, no ChRM directions could be obtained from the remaining of the processed samples due to highly erratic non-interpretable demagnetization paths.

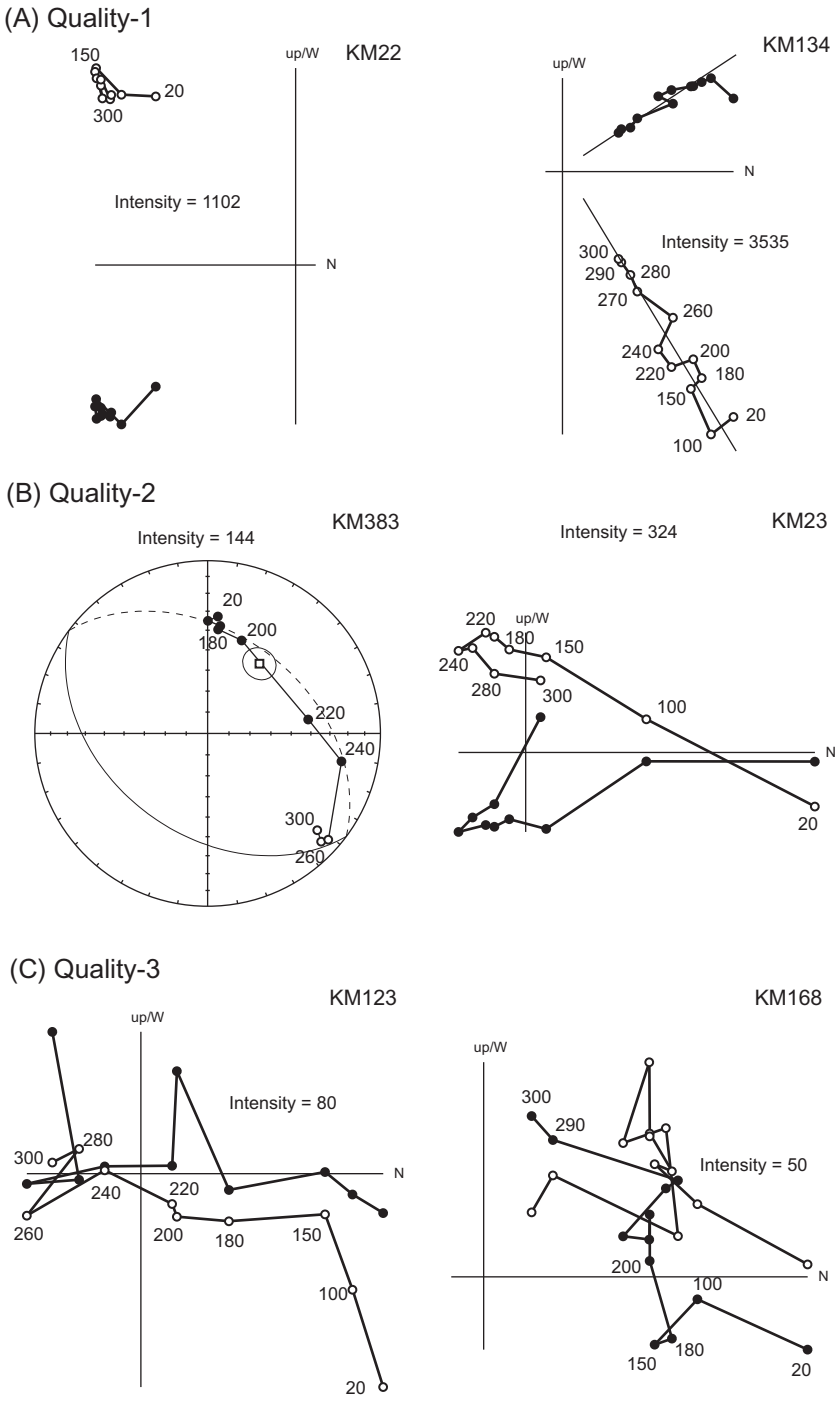


**Fig. 6.** Representative thermal demagnetization diagrams yielding (A) quality-1, (B) quality-2 and (C) rejected quality-3 ChRM directions (see text for discussion). Full symbols are projections on the horizontal plane and open symbols on the vertical plane. Number next to symbol indicates temperature of demagnetization step in °C. The starting intensity is given in $10^{-3}$ A/m. A stereographic projection in (B) shows typical demagnetization path on which great circle analysis was performed (McFadden and McElhinny, 1988).

To assess the primary character of the MTC, field tests were applied to the dataset of obtained quality-1 and quality-2 ChRM directions (Fig. 7). For each section, ChRM directions cluster in antipodal fashion upon tilt correction, suggesting a primary record of normal and reversed polarities. Of these, 25 outlying ChRM directions with virtual geomagnetic poles (VGP) below 30° were systematically discarded. The fold test (Tauxe, 1998) applied to the resulting dataset of both sections is clearly positive with 95% confidence (Fig. 7C), suggesting pre-tectonic magnetization. The reversal test applied to each section (Tauxe, 1998) is positive with 95% confidence (Fig. 7A and B), further suggesting primary magnetization.

We further compared the ChRM directions observed with expected directions from the Apparent Polar Wander Path of India (Torsvik et al., 2008) at the time of deposition. For each section, the mean of combined normal and reverse directions was compared to the expected direction of the magnetic field computed from the pole of India at 10 Ma for section B and 0 Ma for section

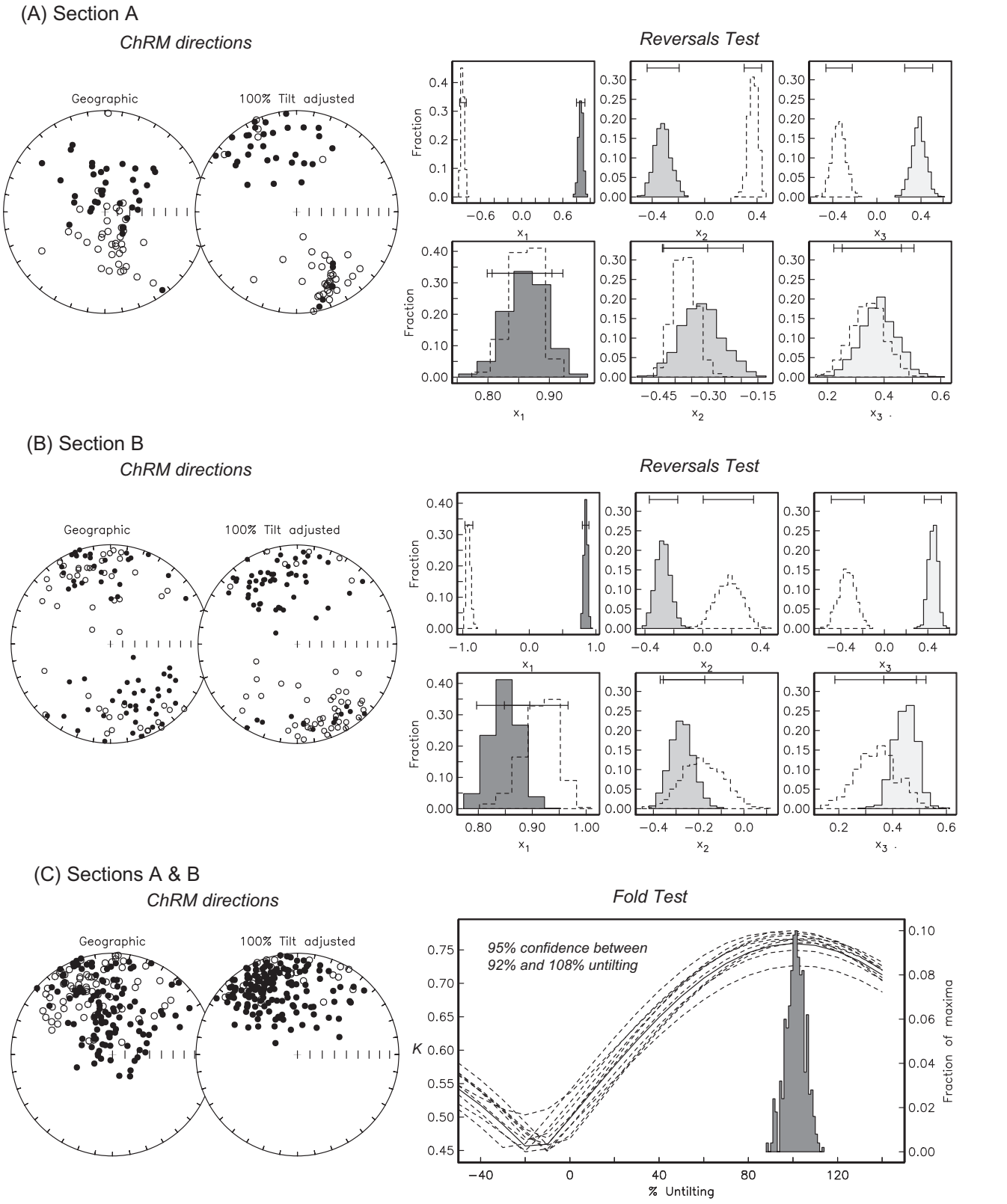


**Fig. 7.** ChRM directions and stability tests for (A) Section A; (B) Section B; (C) the combined data. Left diagrams are stereographic projections of quality-1 and quality-2 ChRM directions before (Geographic) and after a 100% tilt correction. Full symbols indicate positive inclination direction projected on the lower hemisphere; open symbols indicate negative inclination direction projected on the upper hemisphere. ChRM directions of sections A and B pass the reversals test of Tauxe (1998) shown to right. In this test normal and reversed directions are compared in $X_1$, $X_2$, $X_3$ coordinates before (top) and after (bottom) flipping reversed directions into normal coordinates. The test is positive if these directions are indistinguishable at a 95% confidence level such that their 95% confidence intervals overlap as shown on bottom diagrams. Combined ChRM directions of sections A and B (reversed directions have been inverted to normal coordinates for the combined fold test) pass the fold test (Tauxe, 1998) shown in right panel of (C). In this test the geographic directions are progressively untilted using the measured bedding attitude. The test is positive if the directions have a maximum in cluster (K) that includes the 100% untilting distribution with 95% confidence as shown.

**Table 1**
Rotation and flattening calculated from observed vs. expected directions.

| Section | Age (Ma) | Site location | | Observed direction | | | | | Reference pole | | | | Expected $I$ | Expected $D$ | Rotation | Flattening |
|---|---|---|---|---|---|---|---|---|---|---|---|---|---|---|---|---|
| | | Lat. (°N) | Long. (°E) | $I_s$ (°) | $D_s$ (°) | $\alpha_{95}$ (°) | $k$ | $n$ | Age | Lat. (°N) | Long. (°E) | $A_{95}$ (°) | $Ix \pm I$ (°) | $Dx \pm D$ (°) | $R \pm R$ (°) | $F \pm F$ (°) |
| A | 5 | 27.07 | 92.55 | 20.9 | 337.8 | 6.3 | 8 | 72 | 0 | 90 | 180.0 | 0 | 45.6 ± 0.0 | 0.0 ± 0.0 | −22.2 ± 5.4 | 24.7 ± 5.0 |
| B | 10 | 27.07 | 92.55 | 21.4 | 344.2 | 5.7 | 7 | 112 | 15–5 | 88.7 | 251.9 | 3.0 | 44.1 ± 3.8 | 0.5 ± 3.3 | −16.3 ± 5.6 | 22.7 ± 5.5 |

*Note:* Section – sampling section; Age – age of sampled section; Lat. – latitude and Long. – Longitude of sampled section; Observed direction – mean ChRM direction; $I_s$ and $D_s$ –mean inclination and declination in stratigraphic coordinates (after tilt correction); $\alpha_{95}$ – radius of 95% confidence interval; $K$ – precision parameter; $n$ – number of ChRM directions used to calculate the mean; Reference pole – Indian paleomagnetic pole from Apparent Polar Wander Path of Torsvik et al., (2008); Age – age window of considered pole; Lat. and Long. – latitude and longitude of paleomagnetic pole; $A_{95}$ – radius of 95% confidence interval; Expected $I$ and $D$ – inclination and declination expected from the Indian paleomagnetic pole at the sampling location with 95% confidence intervals; Rotation – observed minus expected declination with 95% confidence intervals; Flattening – observed minus expected inclination with 95% confidence intervals.

A (Fig. 7 and Table 1). Results show, at a 95% confidence level, that the mean declination is significantly rotated counter-clockwise, by 22.2 ± 5.4° and 16.3 ± 5.6° for section A and section B, respectively. These results confirm that the ChRM was acquired before tectonic rotation, probably linked to activity of the Tipi and Balukpong thrusts. The tectonic significance of these rotations will be dealt with in the discussion. The observed inclinations are shallower than expected at the latitude of India at the time of deposition, yielding flattening of 24.7 ± 5.0° and 22.7 ± 5.5° for sections A and B respectively.

The cause for this flattening of inclination has already been discussed in paleomagnetic studies of Neogene fluvial deposits in other parts of the Himalayan foreland basin (Tauxe and Kent, 1984; Appel et al., 1991; Gautam and Appel, 1994; Gautam and Rösler, 1999; Gautam and Fujiwara, 2000; Ojha et al., 2009) and should be attributed to the horizontal deposition of detrital particles and/or compaction caused by sedimentary loading before sandstone cementation. Flattening and rotation thus provide further evidence for a primary magnetization of the MTC and the ChRM directions can be confidently used for magnetostratigraphic analysis. The resulting set of 184 quality-1 and quality-2 directions provides reliable paleomagnetic polarity determinations at an average interval of 24 m throughout the sampled section, although some significant gaps are present due to original sampling gaps and the relatively large number of levels with non-interpretable directions.

### 4.3. Constraints from detrital apatite and zircon fission-track data

Fission-track ages of detrital apatite or zircon, when not reset because of heating during deep burial in the basin, indicate the cooling age of the source rocks of the sediment. Therefore, when not reset, the FT age must be older than the depositional age and allows calculating the lag-time, defined as the difference between the time the dated grain cooled below the closure temperature and the time it was deposited in the sedimentary basin (e.g. Garver et al., 1999).

Here we use results from two selected samples of Chirouze (2011) to constrain maximum Siwalik depositional ages in the Kameng section. AFT ages from the uppermost sample (KAM14) in section A give an upper age limit, while the lowermost ZFT age in section B (KAM16) gives a lower limit. Given significant resetting of AFT ages in the LS of Nepal (van der Beek et al., 2006), ZFT was chosen for the lower limit as this system is characterized by higher annealing temperatures and therefore has the least chance of being reset (Fig. 8 and Table 2).

In contrast to the Dafla and Kimin Formations, the Subansiri Formation (MS) at Kameng may contain significant detrital input from the Namche Barwa syntaxis (Cina et al., 2009; Chirouze, 2011), for which detrital geochronometers are expected to show much shorter lag-times due to the extremely rapid exhumation of this massif (Stewart et al., 2008). For this reason, we refrain from using samples from this Formation as constraints on the depositional ages, in the absence of more precise constraints on the variation of lag-time throughout the section. We use in situ $^{40}Ar$–$^{39}Ar$ analysis on micas (Yin et al., 2010) for estimating exhumation rates and thus expected lag times, which have not been constrained previously in the eastern Himalaya. The youngest in situ $^{40}Ar$–$^{39}Ar$ ages were encountered in the vicinity of the MCT and are about 8 Ma. Assuming a constant geothermal gradient between cooling below the $^{40}Ar$–$^{39}Ar$ and FT closure temperature (ZFT and AFT), this zone would produce apatite and zircon with FT lag times on the order of 2.4 Myr and 5 Myr, respectively. In the central Himalaya of Nepal, the Neogene Siwaliks yield lag-time values for the youngest age populations ranging between 1.5 Myr and 2.0 Myr for AFT, and ca. 4.0 Myr for ZFT (van der Beek et al., 2006; Bernet et al., 2006). Theses results fit well with our first-order estimation of lag-times from in situ analysis.

Two AFT age populations have been distinguished in KAM14 with the youngest age-peak at 4.0 Ma (Table 2). This age thus represents the maximum possible depositional age if the lag-time were zero. This age minus the AFT lag-time estimated above provides a more realistic estimate for the lower limit of the depositional age. Therefore, the depositional age of sample KAM14 located in the footwall section most likely ranges between 1.6 and 4.0 Ma. Two ZFT age populations have been determined for sample KAM16 collected in the hanging wall of the Tipi Thrust from the Dafla Formation. From its youngest peak age at 16.3 ± 1.4 Ma, the depositional age of the sample located very close to the base of the section should be younger than 16 Ma, more likely around 11–12 Ma, which thus gives an indication for the lower age limit for our section.

## 5. Correlation to the Paleomagnetic Polarity Time Scale (GPTS)

Polarity zones are defined by at least two consecutive paleomagnetic levels with the same polarity. Isolated levels are considered unreliable and ignored for the correlation. Despite some significant gaps in the sampling, 17 polarity zones (9 normal N1 to N9 and 8 reversed R1 to R8) are identified in Section A and 12 polarity zones (6 normal N1 to N6 and 6 reversed R1 to R6) in section B (Fig. 8). The hanging-wall section B comprises the longest observed normal polarity interval N4 of the entire sampled section and constitutes the starting point of our correlation. Independent constraints from FT data indicate that section B is younger than 16.3 Ma, most likely around 12 Ma. Inspection of the GPTS in this age range indicates the obvious correlation of the longest normal zone of the section N4 with chron C5n.2n, the longest normal polarity chron of the Miocene (Fig. 8). This correlation indicates that the boundary between the Dafla Formation and the Subansiri Formation, located within the polarity zone N4, should have an age of 10–11 Ma, which confirms the regional correlation of these formations to the lower and middle Siwaliks respectively (Ojha et al., 2009). Indeed, the lower to middle Siwaliks boundary has been located within or near C5n.2n in previous magnetostratigraphic studies of the Siwaliks (Ojha et al., 2009).

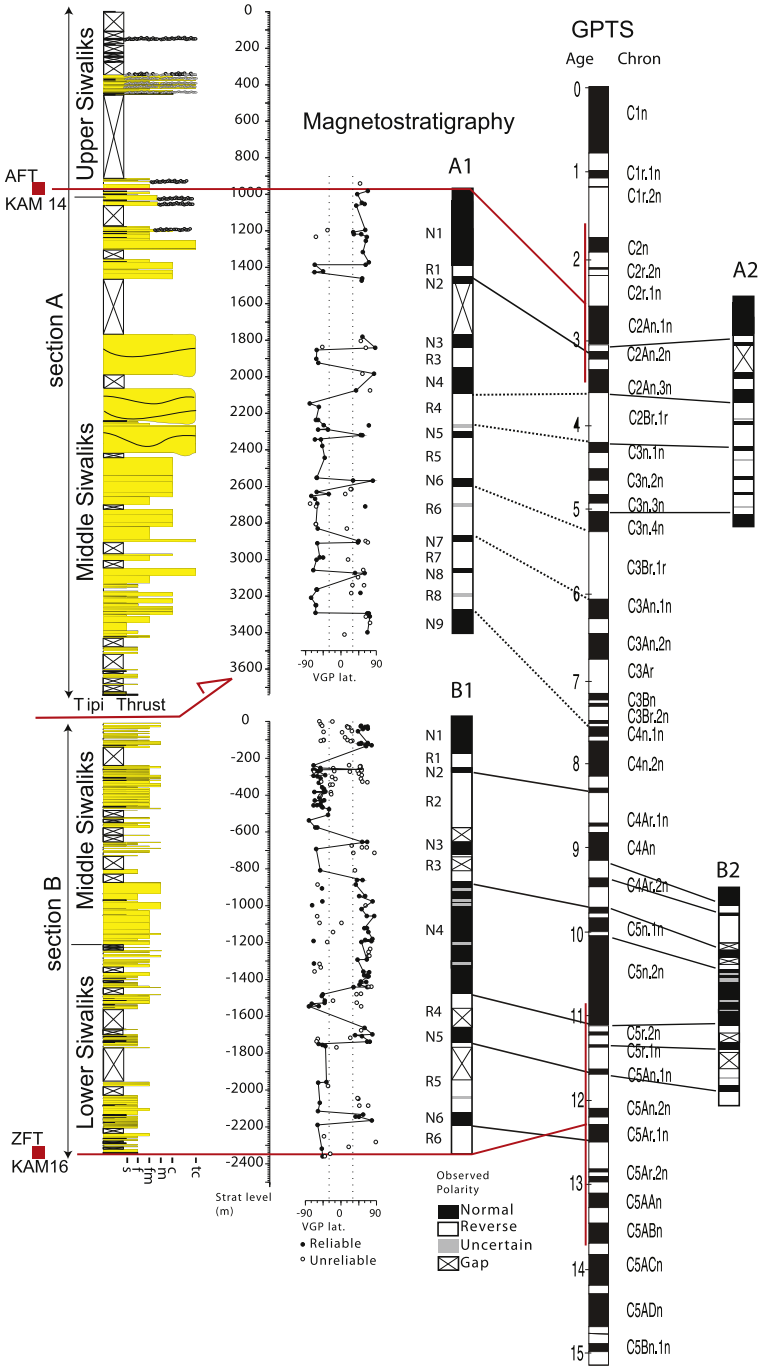


**Fig. 8.** Lithostratigraphy and magnetostratigraphy of the Kameng sections. Solid points in magnetostratigraphy log are virtual geomagnetic pole latitudes (VGP lat.) derived from reliable quality-1 and quality-2 ChRM directions, open points are unreliable quality-3 ChRM directions. Black and white intervals in the polarity columns indicate normal and reverse polarity intervals respectively, defined by at least two reliable ChRM directions of the same polarity; grey intervals indicate unsure polarity defined by only one ChRM direction. Crossed intervals indicate gaps in the sampling. Most probable ages of deposition of FT samples are indicated in red. Preferred correlations (A1 and B1) of the polarity column to the geomagnetic polarity time scale (GPTS) of Lourens et al. (2004) are indicated. Alternative correlations (A2 and B2) are shown on the right. (For interpretation of the references to color in this figure legend, the reader is referred to the web version of this article.)

The footwall section A contains large gaps due to the lack of continuous outcrops for sampling and because this portion of the section is dominated by coarse and sometimes weathered sand that commonly yielded non-interpretable demagnetization diagrams. However, provided the maximum age constraints from our detrital AFT sample (4.0–1.6 Ma, see above), the conspicuous ~400 m thick normal polarity zone N1 at the top of the sampled section is logically correlated with chron C2An.1n. This correlation places the Kimin–Subansiri Formation boundary, located at the top of the sampled section and attributed to the middle to upper Siwaliks transition, at 2.6–3.6 Ma, in excellent agreement with the estimated age of this transition elsewhere along the Himalayan front (Ojha et al., 2009; Fig. 9).

Further correlation of the rest of the polarity zones is not straightforward due to the numerous gaps in the record, so that we propose two possible sets of correlations (Fig. 8). In the set correlations A2 and B2, we assume that a minimum number of chrons have been missed by the observed polarity zones and we obtain a

**Table 2**
Detrital apatite (AFT) and zircon (ZFT) fission-track results, Kameng section, Arunachal Pradesh (from Chirouze, 2011).

| Sample | Analysis | *n* | Age range (Ma) | P1 | | P2 | |
|---|---|---|---|---|---|---|---|
| | | | | (Ma) | (%) | (Ma) | (%) |
| KAM 14 | AFT | 59 | 1.9–106 | 4.0 ± 0.9 | 85.5 | 13.6 ± 7.7 | 14.5 |
| KAM16 | ZFT | 100 | 8.1–400 | 16.3 ± 1.4 | 65.7 | 153.1 ± 21.5 | 34.3 |

*Note:* Sample – Sample identification; Analysis – Apatite Fission-Track or Zircon Fission-Track analysis; *n* – total number of grains counted; Age range – Age range of all counted grains; Pi – Population binomial peak-fit age given with ± 2 Sigma Error (SE). Also given is the percentage of grains in a specific peak. All samples were counted at magnitude 1250x dry (100x objective, 1.25 tube factor, 10 oculars) using a zeta (IRM 540) of 275.32 ± 9.92 (±1 SE) for AFT counting and of 347.14 ± 5.40 (±1 SE) for zircon ZFT counting.

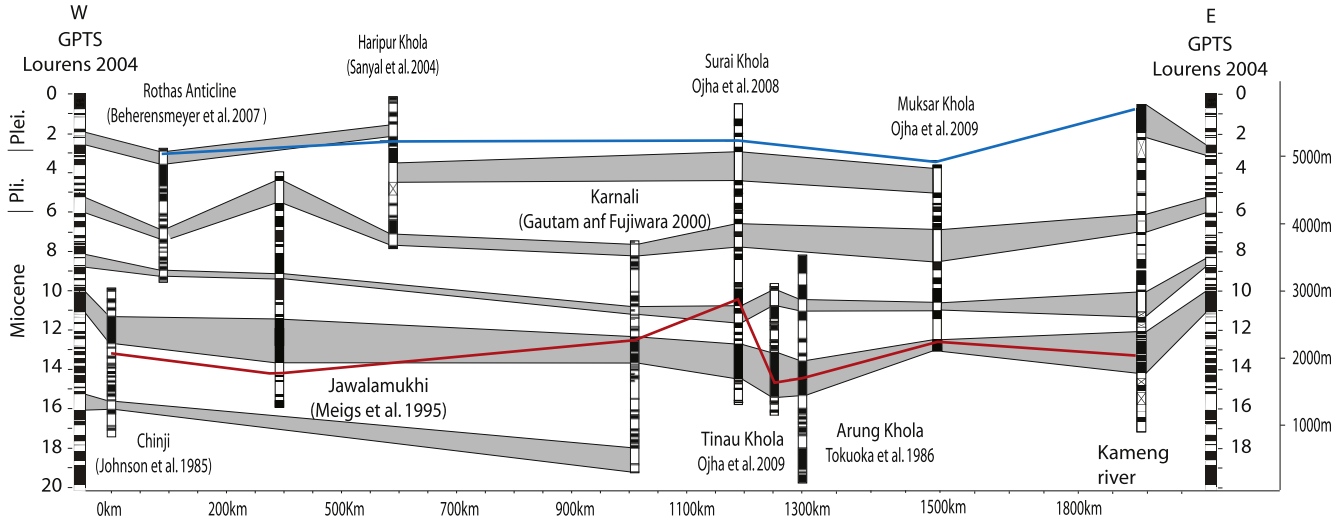


**Fig. 9.** Review of magnetostratigraphic correlations to the GPTS (Lourens et al., 2004) of studied stratigraphic sections of Siwalik deposits along the Himalayan foreland shown as stratigraphic thickness vs. longitudinal distance between sections from West to East (modified from Ojha et al. (2009)). Shaded areas highlight the major correlation intervals. Colored lines indicate the correlation of the Siwalik formation boundaries (red line: lower Siwalik to middle Siwalik transition, blue line: middle Siwalik to upper Siwalik transition). (For interpretation of the references to color in this figure legend, the reader is referred to the web version of this article.)

possible pattern fit with the long dominantly reversed zones R4 and R5 of section A correlated to C2Br.1r. Similarly, the long zone R2 of section B is correlated to C4Ar.2r. These correlations, however, would imply very high accumulation rates of 960 m/Myr and 800 m/Myr for A2 and B2 respectively, which appear unrealistic with respect to rates observed elsewhere along the Himalayan foreland that are in the 180–590 m/Myr range (Figs. 9 and 10). This inconsistency suggests that some of the chrons have been missed by our sampling, which is not exceedingly surprising given the existing gaps.

In the alternative set correlations A1 and B1 we use the same starting points but compare the length of the longest mainly normal polarity zones and the longest mainly reversed zones allowing that some of the chrons have been missed. For section A, N1 remains correlated to C2An.1n but R4 is correlated to the long reversed chron C2Br.1r, N5 to N6 would represent chrons C3n.1n to C3n.4n and R6 is correlated to the long reversed chron C3Br.1r. It would follow that N7 correlates with C3An.1n, R8 with C3Ar and N9 with C4n. For section B, N4 remains correlated to C5n, the long R2 above would correlate to C4Ar.1n and N1 (at the top of the section) is linked to the base of the long C4n.2n. Below N4 the correlation is especially challenging but assuming steady accumulation rates, we can correlate N5 to C5An.1n, R4 to C5An.1r and thus N6 to C5Ar.1n and R6 to C5Ar.1r. These correlations are admittedly tentative but they respect the general observed polarity patterns and imply consistent accumulation rates throughout the section (~440 m/Myr for section B and ~420 m/Myr for section A) that are reasonable for such a foreland context. Another argument in favor of these correlations A1 and B1 is the fact that correlations A2 and B2 imply that a significant portion of Siwalik sediments has been cut off by the Tipi Thrust. This implication is not supported by our sedimentological facies observation at the top of the section B and the bottom of the section A, which are very similar suggesting that only a small part of the Siwalik Group was cut off or possibly even doubled by the Tipi Thrust.

## 6. Discussion

### 6.1. Paleo-environmental implications of the magnetic carrier phase

Our paleomagnetic results indicate a relatively low-temperature (150–340 °C) ChRM yielding reliable primary directions. Rock-magnetic properties suggest the ChRM is carried by an iron sulfide such as greigite. Many earlier studies plead for early diagenetic formation of greigite (Tric et al., 1991; Horng et al., 1992; Mary et al., 1993; Roberts and Turner, 1993; Hallam and Maher, 1994; Maher and Hallam, 2005) or even preserved primary biogenic greigite (Vasiliev et al., 2008), but others argue that caution must be exercised when considering greigite as a paleomagnetic recorder because it frequently grows during later diagenesis (Horng et al., 1998; Dekkers et al., 2000; Roberts and Weaver, 2005; Sagnotti et al., 2005; Rowan and Roberts, 2006). Positive field tests clearly indicate we are dealing with primary magnetization in our case. Furthermore, the typical flattening due to inclination shallowing observed in our samples suggests that the primary

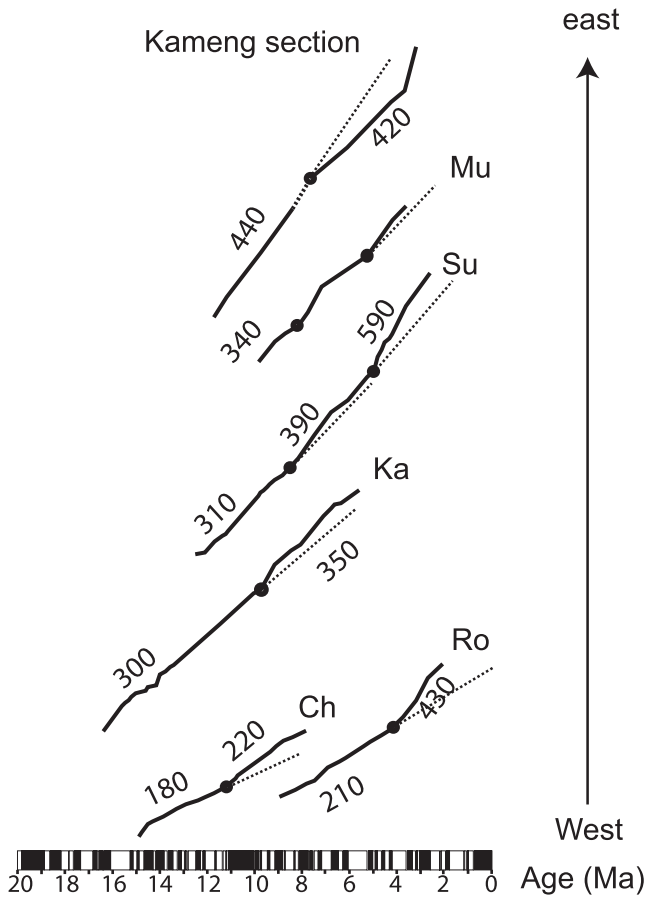


**Fig. 10.** Review of sediment accumulation curves (m/Myr) based on previous magnetostratigraphic studies along the Himalayan foreland plotted against the GPTS of Lourens et al. (2004) and aligned from East (top) to West (bottom). Ch: Chinji (Johnson et al., 1985); Ro: Rohtas Anticline (Behrensmeyer et al., 2007); Ka: Karnali River (Gautam and Fujiwara, 2000); Su: Surai Khola (Ojha et al., 2009); Mu: Muksar Khola (Ojha et al., 2009); Kameng River (this study).

ChRM has been acquired before compaction, probably during early diagenetic processes, similar to other Siwalik magnetostratigraphic records (Tauxe and Kent, 1984; Appel et al., 1991; Gautam and Appel, 1994; Gautam and Rösler, 1999; Gautam and Fujiwara, 2000; Ojha et al., 2000, 2009). We speculate that this early diagenetic formation and preservation of primary iron sulfides, which is not observed in other Siwalik records, is related to the more brackish environment described in the Siwaliks of the far eastern Himalayas of Arunachal Pradesh (Singh and Prakash, 1980; Singh and Tripathi, 1990; Mehrotra et al., 1999), similar to iron sulfide magnetization previously observed in such brackish depositional environments (Jelinowska et al., 1998; Vasiliev et al., 2004, 2008). Joshi et al. (2003) reported typical coastal plant megafossils and cuticular fragments in the upper part of the Kameng section, probably implying that the brackish influence remained even though this part of the section is constituted of coarse sandstone and conglomerate. Thus, it appears that the depositional environment remained brackish throughout deposition of the Kameng section or, alternatively, some brackish or coastal sediments have been recycled from the range or the Brahmaputra plain.

### 6.2. ChRM directions in the Kameng section

Our results show counter-clockwise deviation of the primary ChRM declination of 22.2 ± 5.4° for section A and of 16.3 ± 5.6° for section B with respect to the Indian plate. These rotations are statistically indistinguishable at the 95% confidence level. Section B is in the hanging wall of the Tipi Thrust, while section A is located in the footwall of the Tipi Thrust and constitutes the hanging wall of the MFT zone. The rotation is post-depositional and therefore relatively young. These observations suggest that the ~20° counter-clockwise rotation affected both thrust sheets and is likely to be associated to activity of the underlying MFT zone. The sampling area is located along a marked ~90° bend of both the Tipi Thrust and the MFT zone (Fig. 2). This local structure, possibly associated with a transfer tear fault at depth, provides the simplest explanation for the observed counter-clockwise rotation. However, a regional contribution cannot be completely excluded. Existing paleomagnetic studies have reported systematic ~20° counter-clockwise rotations in the central and western parts of the Himalayan foreland. In Nepal, similar counter-clockwise rotation has been documented in the Siwalik Group of the Khutia Khola (Ojha et al., 2000) and Tinau Khola (Gautam and Appel, 1994) sections. In fact ~20° counter-clockwise rotations are also noted as far west as the Potwar area in northern Pakistan (Opdyke et al., 1982). Our results show that the regional consistency of these rotations extends along the arc from the western to the eastern Himalayas and may thus result from a broader tectonic mechanism. Systematic local counter-clockwise rotations of thrust sheets along the arc are consistent with partitioning of arc-normal and left-lateral strain. Such partitioning may result from accommodating the counter-clockwise swing from west to east along the arc of the convergence axis as evidenced by earthquake focal mechanisms and GPS data (Molnar and Lyon Caen, 1989; Paul et al., 2001).

### 6.3. Evolution of the eastern Himalayan foreland

As in the other parts of the Himalaya, the Siwalik sequence in the far eastern Himalaya coarsens upward and comprises dominantly fluvial deposits with a trend to more proximal facies through time. Despite these general similarities, four interesting peculiarities may be outlined.

First, accumulation rates calculated along the Kameng River section, which range from 420 m/Ma to 440 m/Ma, are slightly higher than those calculated in central Nepal and Pakistan (Johnson et al., 1985; Gautam and Appel, 1994; Ojha et al., 2009) (Fig. 10). Note that these rates result from our more conservative correlation 1; we therefore consider the difference in rates robust despite imprecision in the details of the correlations of sections A and B. Surprisingly, the overall tendency of the sedimentation rates along the Kameng section is to decrease upsection from about 8 Ma, whereas they increase in the rest of the Neogene Himalayan foreland basin. In detail, an increase in sedimentation rate may occur at the MS-US transition, but this is only defined by one correlation and should not be over-interpreted. Within a foreland basin, the rate of subsidence is expected to increase through time as the elastic flexural wave migrates toward the foreland (Angevine et al., 1990). Such a pattern has been demonstrated in many foreland basins (e.g. Angevine et al., 1990; DeCelles and Currie, 1996; Tensi et al., 2006). In all the sections from Pakistan, western Himalaya and Nepal, accumulation rate curves exhibit upward concavity, but this is not obvious from the Kameng section.

Second, the Kameng section appears to be somewhat thicker than correlative sections further west (Fig. 9; Johnson et al., 1985; Gautam and Fujiwara, 2000; Ojha et al., 2009). The total thickness of the Siwalik Group along the Kameng section is difficult to estimate because of the doubling or cut-off that could be due to the Tipi Thrust. Our magnetostratigraphy suggests that the upper part of the hanging-wall section and the lower part of footwall section both correlate to the normal chron C4n.2n (Fig. 8). Assuming a constant 440 m/Myr deposition rate during the time covered by this chron, it follows that a small part (~350 m) of the section may be doubled, reducing its thickness from 6.1 to 5.8 km. Total

**Table A1**
DR1A. ChRM direction of section A.

| Spl ID | Level (m) | $D_g$ (°) | $I_g$ (°) | $D_s$ (°) | $I_s$ (°) | MAD (°) | VGP (°N) | Q | Dip az. (°N) | Dip (°) |
|---|---|---|---|---|---|---|---|---|---|---|
| 362 | −981.2 | 51.4 | 36.8 | 16.6 | 23.1 | 2.8 | 68.4 | 1 | 226.5 | 56.0 |
| 365 | −999.1 | 285.5 | 79.0 | 310.3 | 24.4 | 5.0 | 41.5 | 1 | 226.5 | 56.0 |
| 368 | −1047.1 | 350.6 | 75.9 | 325.0 | 22.0 | 8.1 | 53.6 | 1 | 226.5 | 56.0 |
| 369 | −1053.5 | 2.1 | 54.9 | 341.0 | 7.1 | 6.3 | 60.3 | 1 | 226.5 | 56.0 |
| 372 | −1061.5 | 272.2 | 78.3 | 307.5 | 25.3 | 7.2 | 39.2 | 1 | 226.5 | 56.0 |
| 334 | −1195.3 | 59.9 | 76.1 | 333.1 | 28.1 | 4.6 | 62.2 | 1 | 227.7 | 64.0 |
| 337 | −1207.1 | 287.1 | 64.1 | 304.8 | 3.2 | 6.1 | 31.4 | 1 | 227.7 | 64.0 |
| 338 | −1218.1 | 1.9 | −2.8 | 26.5 | −41.7 | 7.9 | 32.9 | 1 | 227.7 | 64.0 |
| 339 | −1218.9 | 349.2 | 72.5 | 326.9 | 10.8 | 2.7 | 51.8 | 1 | 227.7 | 64.0 |
| 340 | −1233.6 | 48.2 | 36.0 | 14.7 | 15.3 | 4.3 | 66.2 | 1 | 227.7 | 64.0 |
| 342 | −1254.4 | 20.1 | 48.2 | 354.0 | 2.8 | 3.4 | 63.7 | 1 | 227.7 | 64.0 |
| 344 | −1316.0 | 1.3 | 66.4 | 333.9 | 8.1 | 6.9 | 56.1 | 1 | 227.7 | 64.0 |
| 347 | −1372.5 | 41.1 | 55.4 | 354.0 | 17.6 | 3.2 | 71.1 | 1 | 227.7 | 64.0 |
| 348 | −1385.6 | 105.7 | 71.5 | 330.6 | 41.1 | 6.6 | 63.3 | 1 | 227.7 | 64.0 |
| 349 | −1385.9 | 210.6 | −61.5 | 165.9 | −15.0 | 2.0 | −66.4 | 1 | 227.7 | 64.0 |
| 351 | −1422.5 | 158.7 | −41.7 | 154.2 | 19.6 | 18.4 | −45.2 | 1 | 227.7 | 64.0 |
| 352 | −1426.9 | 276.3 | −69.7 | 155.2 | −40.2 | 2.8 | −67.2 | 1 | 227.7 | 64.0 |
| 354 | −1460.7 | 354.4 | 57.5 | 336.4 | −1.0 | 4.8 | 54.3 | 1 | 227.7 | 64.0 |
| 357 | −1472.7 | 354.3 | 72.7 | 328.1 | 11.8 | 3.8 | 53.0 | 1 | 227.7 | 64.0 |
| 374 | −1779.9 | 344.3 | 51.3 | 335.1 | 2.2 | 5.4 | 54.7 | 1 | 230.5 | 51.5 |
| 380 | −1840.6 | 71.6 | 60.8 | 358.9 | 42.9 | 4.1 | 87.6 | 1 | 230.5 | 51.5 |
| 381 | −1853.2 | 183.6 | −43.4 | 170.3 | −0.7 | 24.3 | −61.7 | 2 | 230.5 | 51.5 |
| 383 | −1901.1 | 186.9 | −72.2 | 154.7 | −25.3 | 20.2 | −62.6 | 2 | 230.5 | 51.5 |
| 385 | −1923.5 | 167.9 | −63.3 | 152.8 | −14.1 | 18.0 | −57.4 | 2 | 230.5 | 51.5 |
| 389 | −1983.6 | 86.1 | 63.4 | 354.6 | 49.5 | 5.5 | 84.2 | 1 | 230.5 | 51.5 |
| 290 | −2074.1 | 297.8 | 62.6 | 310.3 | 12.5 | 5.2 | 38.5 | 2 | 231.0 | 51.8 |
| 293 | −2146.5 | 228.7 | −61.3 | 175.4 | −31.8 | 4.2 | −79.3 | 2 | 231.0 | 51.8 |
| 295 | −2164.5 | 238.3 | −27.7 | 212.4 | −22.1 | 15.7 | −55.8 | 2 | 231.0 | 51.8 |
| 298 | −2236.1 | 187.8 | −69.4 | 157.2 | −22.9 | 3.0 | −63.8 | 2 | 231.0 | 51.8 |
| 299 | −2236.7 | 171.1 | −74.2 | 149.6 | −24.2 | 6.0 | −58.1 | 2 | 231.0 | 51.8 |
| 300 | −2265.3 | 70.1 | −80.3 | 129.9 | −34.5 | 6.5 | −43.5 | 2 | 231.0 | 51.8 |
| 301 | −2265.8 | 34.9 | 46.6 | 4.8 | 17.4 | 6.6 | 71.3 | 2 | 231.0 | 51.8 |
| 303 | −2289.5 | 145.8 | −16.4 | 146.6 | 35.2 | 6.7 | −33.3 | 2 | 231.0 | 51.8 |
| 302 | −2289.5 | 175.8 | −41.3 | 166.5 | 4.4 | 1.8 | −58.0 | 2 | 231.0 | 51.8 |
| 304 | −2319.0 | 316.0 | 78.6 | 319.9 | 26.8 | 5.6 | 50.5 | 1 | 231.0 | 51.8 |
| 305 | −2319.9 | 141.0 | 67.5 | 321.0 | 60.7 | 10.1 | 55.0 | 2 | 231.0 | 51.8 |
| 307 | −2343.2 | 148.5 | −66.4 | 144.1 | −14.8 | 4.8 | −50.8 | 2 | 231.0 | 51.8 |
| 306 | −2343.2 | 190.5 | −59.4 | 164.7 | −15.8 | 4.6 | −66.1 | 2 | 231.0 | 51.8 |
| 309 | −2378.2 | 135.5 | −68.7 | 138.9 | −17.0 | 17.1 | −47.1 | 2 | 231.0 | 51.8 |
| 312 | −2443.9 | 128.2 | −49.8 | 131.8 | −17.2 | 14.8 | −41.0 | 2 | 229.3 | 33.0 |
| 314 | −2553.0 | 162.3 | −61.1 | 151.8 | −29.5 | 9.5 | −61.5 | 2 | 229.3 | 33.0 |
| 315 | −2553.9 | 161.3 | −63.2 | 150.7 | −31.4 | 3.3 | −61.1 | 1 | 229.3 | 33.0 |
| 316 | −2568.0 | 307.8 | 22.5 | 308.5 | −9.9 | 3.8 | 30.8 | 1 | 229.3 | 33.0 |
| 317 | −2568.9 | 56.8 | 60.3 | 8.9 | 49.8 | 3.3 | 81.4 | 1 | 229.3 | 33.0 |
| 322 | −2630.6 | 165.3 | −45.7 | 157.8 | −15.0 | 4.7 | −61.4 | 2 | 229.3 | 33.0 |
| 325 | −2641.9 | 143.7 | 4.9 | 144.9 | 37.8 | 4.9 | −31.0 | 1 | 229.3 | 33.0 |
| 326 | −2653.2 | 241.6 | −56.4 | 196.1 | −49.7 | 6.2 | −75.5 | 1 | 229.3 | 33.0 |
| 329 | −2668.8 | 170.6 | −54.9 | 158.5 | −24.7 | 24.1 | −65.4 | 2 | 229.3 | 33.0 |
| 331 | −2694.8 | 165.3 | −38.9 | 159.5 | −8.4 | 26.1 | −59.9 | 2 | 229.3 | 33.0 |
| 332 | −2709.8 | 345.4 | 48.6 | 337.1 | 17.8 | 11.2 | 61.9 | 1 | 229.3 | 33.0 |
| 244 | −2807.3 | 133.6 | −71.7 | 156.1 | −24.2 | 13.0 | −63.4 | 2 | 257.0 | 50.0 |
| 246 | −2831.5 | 63.7 | −73.8 | 145.7 | −41.8 | 13.7 | −59.0 | 2 | 257.0 | 50.0 |
| 248 | −2899.5 | 331.3 | 30.6 | 332.8 | −17.9 | 4.3 | 45.2 | 2 | 257.0 | 50.0 |
| 251 | −2907.8 | 305.5 | 45.3 | 319.2 | 3.1 | 8.4 | 43.3 | 2 | 257.0 | 50.0 |
| 252 | −2912.0 | 109.8 | −72.3 | 150.0 | −29.1 | 21.2 | −59.9 | 2 | 257.0 | 50.0 |
| 254 | −2989.1 | 162.3 | −39.2 | 163.3 | 10.7 | 14.7 | −53.7 | 2 | 257.0 | 50.0 |
| 255 | −2989.9 | 153.7 | −29.3 | 154.7 | 19.6 | 23.9 | −45.5 | 2 | 257.0 | 50.0 |
| 257 | −3001.9 | 130.7 | −70.8 | 154.7 | −23.8 | 18.8 | −62.1 | 2 | 257.0 | 50.0 |
| 259 | −3058.9 | 18.1 | −85.2 | 159.0 | −55.4 | 17.2 | −70.1 | 2 | 253.8 | 38.5 |
| 261 | −3075.1 | 250.2 | 59.4 | 299.0 | 43.9 | 4.7 | 35.9 | 2 | 253.8 | 38.5 |
| 260 | −3075.7 | 57.6 | 49.3 | 29.3 | 28.7 | 7.8 | 60.4 | 2 | 253.8 | 38.5 |
| 266 | −3165.5 | 342.1 | −72.1 | 165.3 | −69.4 | 4.7 | −61.8 | 2 | 253.8 | 38.5 |
| 267 | −3166.8 | 85.6 | −78.4 | 146.7 | −47.8 | 9.2 | −60.6 | 2 | 253.8 | 38.5 |
| 268 | −3184.0 | 334.2 | 27.4 | 335.1 | −10.6 | 5.0 | 49.6 | 2 | 253.8 | 38.5 |
| 270 | −3210.8 | 166.1 | −82.7 | 164.2 | −44.2 | 1.9 | −75.8 | 2 | 253.8 | 38.5 |
| 272 | −3250.7 | 154.5 | −56.2 | 158.4 | −18.0 | 8.6 | −62.9 | 2 | 253.8 | 38.5 |
| 273 | −3251.5 | 152.6 | −60.7 | 157.9 | −22.6 | 16.8 | −64.2 | 2 | 253.8 | 38.5 |
| 276 | −3293.0 | 160.7 | −54.4 | 161.9 | −15.9 | 24.5 | −64.4 | 2 | 253.8 | 38.5 |
| 278 | −3295.8 | 322.9 | 80.5 | 339.2 | 42.5 | 6.3 | 71.1 | 2 | 253.8 | 38.5 |
| 279 | −3296.1 | 343.1 | 58.2 | 343.4 | 19.7 | 3.5 | 67.0 | 2 | 253.8 | 38.5 |
| 282 | −3313.3 | 80.6 | 67.8 | 18.5 | 48.8 | 4.7 | 73.5 | 2 | 253.8 | 38.5 |
| 287 | −3399.7 | 131.2 | 70.7 | 9.6 | 65.8 | 8.8 | 67.7 | 2 | 253.8 | 38.5 |

(*continued on next page*)

**Table A1** (*continued*)

| Spl ID | Level (m) | $D_g$ (°) | $I_g$ (°) | $D_s$ (°) | $I_s$ (°) | MAD (°) | VGP (°N) | Q | Dip az. (°N) | Dip (°) |
|---|---|---|---|---|---|---|---|---|---|---|
| *Rejected ChRM directions* | | | | | | | | | | |
| 361 | −941.2 | 348.7 | 24.0 | 348.8 | −24.4 | 13.7 | 48.7 | 3 | 226.5 | 56.0 |
| 335 | −1195.9 | 128.8 | −54.6 | 132.5 | 9.0 | 14.6 | −34.3 | 3 | 227.7 | 64.0 |
| 341 | −1233.1 | 225.1 | −72.8 | 156.6 | −24.0 | 7.6 | −63.7 | 3 | 227.7 | 64.0 |
| 376 | −1803.7 | 326.1 | 72.4 | 322.3 | 21.0 | 9.6 | 51.1 | 3 | 230.5 | 51.5 |
| 377 | −1836.8 | 144.9 | −58.3 | 142.8 | −6.9 | 11.4 | −47.3 | 3 | 230.5 | 51.5 |
| 379 | −1840.9 | 27.3 | 78.6 | 333.1 | 33.3 | 15.3 | 63.7 | 3 | 230.5 | 51.5 |
| 388 | −1983.1 | 339.4 | 77.5 | 325.0 | 26.6 | 9.7 | 54.9 | 3 | 230.5 | 51.5 |
| 291 | −2074.8 | 43.3 | 68.9 | 346.1 | 32.6 | 9.4 | 74.1 | 3 | 231.0 | 51.8 |
| 320 | −2615.0 | 245.5 | 68.0 | 288.0 | 46.1 | 12.0 | 27.0 | 1 | 229.3 | 33.0 |
| 321 | −2615.4 | 92.7 | 24.5 | 73.6 | 43.5 | 5.6 | 25.0 | 2 | 229.3 | 33.0 |
| 324 | −2641.9 | 307.6 | −16.1 | 302.3 | −48.2 | 7.4 | 11.1 | 2 | 229.3 | 33.0 |
| 330 | −2694.8 | 210.1 | −48.6 | 185.9 | −30.7 | 13.5 | −78.1 | 3 | 229.3 | 33.0 |
| 333 | −2709.8 | 165.5 | −56.3 | 155.0 | −25.2 | 29.7 | −62.8 | 3 | 229.3 | 33.0 |
| 245 | −2807.3 | 122.8 | −74.5 | 154.8 | −28.2 | 16.8 | −63.6 | 3 | 257.0 | 50.0 |
| 247 | −2831.5 | 21.1 | −15.9 | 47.7 | −51.8 | 4.8 | 15.2 | 2 | 257.0 | 50.0 |
| 249 | −2899.5 | 354.2 | 52.4 | 351.4 | 2.6 | 14.2 | 62.9 | 3 | 257.0 | 50.0 |
| 250 | −2907.8 | 4.3 | 60.8 | 355.5 | 11.8 | 8.2 | 68.5 | 3 | 257.0 | 50.0 |
| 256 | −3001.0 | 224.0 | 40.5 | 277.0 | 47.3 | 5.3 | 18.2 | 2 | 257.0 | 50.0 |
| 258 | −3058.2 | 343.9 | 34.7 | 343.9 | −3.8 | 2.4 | 57.1 | 3 | 253.8 | 38.5 |
| 262 | −3097.6 | 287.1 | 55.7 | 311.9 | 27.0 | 7.0 | 43.5 | 3 | 253.8 | 38.5 |
| 263 | −3097.6 | 202.0 | −67.1 | 180.3 | −32.0 | 12.7 | −80.3 | 3 | 253.8 | 38.5 |
| 264 | −3141.3 | 288.0 | 35.7 | 300.8 | 9.9 | 8.3 | 29.6 | 2 | 253.8 | 38.5 |
| 265 | −3141.8 | 84.5 | 56.4 | 34.9 | 45.7 | 6.3 | 59.0 | 3 | 253.8 | 38.5 |
| 269 | −3184.8 | 322.8 | −2.4 | 316.9 | −37.8 | 2.2 | 26.2 | 2 | 253.8 | 38.5 |
| 283 | −3314.2 | 272.9 | 80.3 | 330.2 | 47.5 | 13.2 | 63.7 | 3 | 253.8 | 38.5 |
| 284 | −3347.5 | 122.5 | 75.0 | 4.7 | 61.3 | 5.9 | 74.2 | 3 | 253.8 | 38.5 |
| 288 | −3411.7 | 138.6 | 34.7 | 106.9 | 65.3 | 2.9 | 9.2 | 3 | 253.8 | 38.5 |

thickness variations are not only caused by changes in basin dynamics, but could also be explained by the structural position of the Balukpong thrust or heterogeneous erosion of the US. It is thus more appropriate to compare the thickness of the MS, which is bounded by conformable stratigraphic contacts. This thickness is about 3600 m along the Kameng River, significantly higher than the thickness of the MS in Nepal. Nepali sections that exhibit continuous outcrop of MS strata provide a thickness ranging between 2500 and 2200 m (Muksar and Surai sections; Ojha et al., 2009).

Third, the main facies transition observed along the Kameng section occurs at 10.5 Ma for the Dafla (LS) to Subansiri (MS) Formations and at 2.6 Ma for the Subansiri (MS) to Kimin (US) Formations. A compilation of pre-existing magnetostratigraphic correlations in the Neogene Himalayan foreland basin in Nepal and Pakistan (Figs. 9 and 10) shows that the main facies transitions between the LS and MS formations occurred at 10.5 ± 0.5 Ma, except at Surai Khola (Ojha et al., 2009; Johnson et al., 1985; Gautam and Fujiwara, 2000). The MS to US transition occurred between 3 and 4.6 Ma in central Nepal (Ojha et al., 2009; Sanyal et al., 2004) and at about 2 Ma in Pakistan (Behrensmeyer et al., 2007). Nonetheless, the time of deposition of the middle Siwaliks appears to have been longer in the eastern (~8 Myr) than in the western Himalayan foreland (3–6 Myr).

Finally, our sedimentological observations argue for an upward reduction of flood-plain facies in the Subansiri (MS) Formation. This reduction occurred contemporaneously with the deposition of thick amalgamated channels of very coarse sand. The US sequence exhibits well-preserved mudstone layers between the conglomerates. These observations suggest sediment by-pass during deposition of the MS which could be due to a variation of the energy of the fluvial system.

These characteristics of the eastern Himalayan foreland basin could be explained by the particular geography of this part of the basin, which is bounded by the Shillong Plateau to the south. In a typical overfilled basin, variations in sedimentation rate can be attributed to variations in subsidence rate, caused by an increase or decrease of the Indian plate elastic flexure (Burbank et al., 1996). However, in the eastern part of the Himalayas, it is difficult to envisage that Indian plate flexure is controlled by elastic deformation alone, as it presents significantly shorter wavelengths than in the central Himalaya (Bilham et al., 2003). Below the Shillong Plateau, which began to be uplifted and exhumed between 13 and 8 Ma (Biswas et al., 2007; Clark and Bilham, 2008), the Moho presents a 5-km offset (Mitra et al., 2005). This apparently brittle behavior of the Indian slab may explain the seemingly constant sedimentation rate along the Kameng section. As a consequence of Shillong Plateau uplift, the braided Brahmaputra River has been forced to flow closer to the Himalayan front than the Ganges River in the central Himalaya, which is still the present-day situation (Fig. 1). Because of this drainage organization in the eastern Himalayan foreland basin, sandy sediments were deposited during a longer period than in the central part, and could explain the important thickness of the MS observed in the Kameng section and the presence of Brahmaputra sediments in the upper part of the Subansiri Formation as mentioned by Cina et al. (2009). We also note that there is no strict relationship between the quantity of sediments carried by the Brahmaputra, which should have strongly increased since 10 Ma due to rapid exhumation in the Eastern Syntaxis (Singh and France-Lanord, 2002; Stewart et al., 2008), and the sedimentation rate, which decreased during this period. This strongly suggests that sedimentation rates in the eastern Himalayan foreland basin are controlled by subsidence rather than by sediment flux.

## 7. Conclusions

Magnetostratigraphic analyses in combination with FT dating of detrital apatite and zircon show that the Siwalik Group in Arunachal Pradesh was deposited between 13 and 2.5 Ma. Our paleomagnetic results and rock magnetic analyses indicate a relatively low temperature ChRM component (150–340 °C) yielding reliable primary directions carried by an iron sulfide like greigite. Despite

**Table A2**
DR1B. ChRM direction of section B.

| Spl ID | Level (m) | $D_g$ (°) | $I_g$ (°) | $D_s$ (°) | $I_s$ (°) | MAD (°) | VGP (°N) | Q | Dip az. (°N) | Dip (°) |
|---|---|---|---|---|---|---|---|---|---|---|
| 91 | −23.0 | 37.2 | −77.6 | 26.1 | −3.9 | 7.1 | 51.6 | 2 | 203.1 | 74.1 |
| 90 | −26.2 | 305.5 | −34.5 | 329.5 | 0.9 | 1.2 | 50.4 | 1 | 203.1 | 74.1 |
| 88 | −27.1 | 1.9 | −6.2 | 337.9 | 59.5 | 14.0 | 67.4 | 2 | 203.1 | 74.1 |
| 86 | −29.3 | 334.3 | −24.3 | 332.4 | 27.7 | 4.7 | 61.5 | 1 | 203.1 | 74.1 |
| 83 | −38.8 | 338.7 | −31.4 | 341.3 | 26.4 | 11.5 | 68.2 | 1 | 203.1 | 74.1 |
| 82 | −41.0 | 328.8 | −21.8 | 326.9 | 24.8 | 2.3 | 56.0 | 1 | 203.1 | 74.1 |
| 81 | −52.4 | 312.3 | −17.6 | 315.8 | 12.6 | 5.2 | 43.2 | 2 | 203.1 | 74.1 |
| 67 | −116.6 | 343.0 | −20.8 | 339.4 | 30.6 | 6.5 | 68.2 | 2 | 198.4 | 62.2 |
| 68 | −116.8 | 339.0 | 1.1 | 316.8 | 43.8 | 9.3 | 51.4 | 2 | 198.4 | 62.2 |
| 65 | −120.6 | 325.3 | −16.4 | 322.5 | 22.2 | 3.1 | 51.6 | 2 | 198.4 | 62.2 |
| 66 | −120.8 | 328.2 | −3.8 | 313.3 | 32.3 | 10.2 | 46.0 | 2 | 198.4 | 62.2 |
| 63 | −128.4 | 355.2 | −28.9 | 355.1 | 29.1 | 2.2 | 77.6 | 2 | 198.4 | 62.2 |
| 64 | −128.4 | 336.8 | −19.5 | 333.3 | 27.9 | 3.0 | 62.3 | 2 | 198.4 | 62.2 |
| 61 | −133.4 | 11.8 | −52.0 | 14.3 | 10.0 | 11.9 | 64.1 | 2 | 198.4 | 62.2 |
| 59 | −237.9 | 200.6 | 7.4 | 202.2 | −54.7 | 5.8 | −69.4 | 2 | 198.4 | 62.2 |
| 55 | −252.7 | 137.1 | 29.4 | 147.9 | −8.1 | 15.6 | −51.7 | 2 | 198.4 | 62.2 |
| 53 | −260.0 | 339.0 | 5.5 | 311.9 | 46.5 | 5.7 | 47.6 | 1 | 198.4 | 62.2 |
| 54 | −260.4 | 308.1 | −71.0 | 359.3 | −20.1 | 7.7 | 52.6 | 2 | 198.4 | 62.2 |
| 52 | −262.3 | 166.4 | 39.0 | 172.9 | −16.8 | 24.4 | −70.3 | 2 | 198.4 | 62.2 |
| 51 | −262.6 | 157.7 | 33.1 | 163.4 | −17.9 | 20.7 | −66.2 | 2 | 198.4 | 62.2 |
| 50 | −264.1 | 120.3 | 68.2 | 175.4 | 21.4 | 15.5 | −51.6 | 2 | 198.4 | 62.2 |
| 45 | −270.7 | 149.0 | 25.1 | 151.8 | −18.9 | 7.2 | −58.2 | 2 | 198.4 | 62.2 |
| 41 | −290.8 | 132.3 | 12.3 | 131.1 | −14.5 | 30.0 | −39.7 | 2 | 198.4 | 62.2 |
| 40 | −294.7 | 162.2 | 34.8 | 167.6 | −18.7 | 25.9 | −69.0 | 2 | 198.4 | 62.2 |
| 39 | −297.5 | 145.0 | 42.1 | 161.7 | −4.5 | 20.1 | −59.6 | 2 | 198.4 | 62.2 |
| 36 | −308.1 | 133.5 | 34.4 | 150.0 | −2.6 | 26.9 | −51.4 | 2 | 198.4 | 62.2 |
| 29 | −332.7 | 143.6 | 29.6 | 151.8 | −12.3 | 23.5 | −56.0 | 2 | 198.4 | 62.2 |
| 26 | −357.0 | 227.2 | 43.2 | 219.6 | −14.2 | 13.5 | −47.5 | 2 | 198.4 | 62.2 |
| 23 | −366.2 | 160.3 | −11.2 | 125.7 | −50.7 | 5.4 | −42.9 | 2 | 198.4 | 62.2 |
| 22 | −380.6 | 119.2 | 25.7 | 136.0 | 3.0 | 2.4 | −38.9 | 1 | 198.4 | 62.2 |
| 21 | −382.3 | 169.1 | 49.8 | 179.8 | −8.1 | 7.6 | −67.0 | 2 | 198.4 | 62.2 |
| 20 | −383.4 | 128.4 | 25.3 | 140.0 | −4.2 | 6.1 | −44.3 | 1 | 198.4 | 62.2 |
| 14 | −413.3 | 142.4 | 51.9 | 169.6 | 13.8 | 16.2 | −54.5 | 2 | 203.3 | 52.7 |
| 12 | −427.1 | 119.2 | 38.1 | 147.9 | 18.0 | 14.9 | −42.2 | 2 | 203.3 | 52.7 |
| 11 | −428.2 | 162.2 | 18.3 | 160.9 | −22.3 | 22.6 | −66.3 | 2 | 203.3 | 52.7 |
| 10 | −432.8 | 216.6 | 54.0 | 211.1 | 2.0 | 5.6 | −49.0 | 2 | 203.3 | 52.7 |
| 8 | −448.9 | 156.9 | −5.4 | 138.7 | −37.1 | 1.8 | −51.9 | 1 | 203.3 | 52.7 |
| 7 | −453.9 | 161.5 | 2.1 | 149.1 | −34.8 | 4.6 | −60.6 | 2 | 203.3 | 52.7 |
| 5 | −454.9 | 167.0 | 29.3 | 171.0 | −15.2 | 4.1 | −68.9 | 1 | 203.3 | 52.7 |
| 3 | −460.4 | 147.1 | 4.4 | 138.9 | −23.3 | 5.3 | −48.7 | 1 | 203.3 | 52.7 |
| 2 | −465.9 | 221.3 | 4.4 | 229.2 | −45.1 | 8.2 | −46.4 | 2 | 203.3 | 52.7 |
| 393 | −475.9 | 131.4 | −1.0 | 115.4 | −32.0 | 4.5 | −30.0 | 1 | 183.0 | 57.0 |
| 395 | −507.1 | 247.8 | −29.0 | 247.2 | −53.0 | 7.2 | −32.6 | 2 | 249.0 | 24.0 |
| 397 | −536.9 | 202.9 | −42.7 | 178.7 | −55.8 | 9.9 | −80.7 | 2 | 249.0 | 24.0 |
| 398 | −575.3 | 182.1 | −10.7 | 176.1 | −4.3 | 21.6 | −64.8 | 2 | 277.0 | 44.0 |
| 399 | −575.5 | 172.1 | −26.8 | 158.0 | −9.5 | 7.3 | −59.4 | 2 | 277.0 | 44.0 |
| 400 | −653.0 | 1.0 | 52.4 | 322.5 | 31.7 | 6.2 | 54.0 | 2 | 277.0 | 44.0 |
| 401 | −653.2 | 10.1 | 7.7 | 3.8 | 7.7 | 4.4 | 66.5 | 2 | 277.0 | 44.0 |
| 125 | −691.5 | 158.8 | 29.4 | 162.8 | −9.5 | 3.2 | −62.3 | 2 | 190.0 | 44.0 |
| 181 | −807.9 | 154.0 | 44.1 | 175.6 | 20.2 | 21.9 | −52.3 | 2 | 220.0 | 40.0 |
| 182 | −859.9 | 40.3 | 10.5 | 40.4 | 50.5 | 15.2 | 54.7 | 2 | 220.0 | 40.0 |
| 183 | −860.1 | 47.0 | −30.1 | 46.1 | 9.7 | 8.6 | 40.8 | 2 | 220.0 | 40.0 |
| 184 | −884.6 | 8.8 | 50.1 | 297.5 | 70.1 | 9.6 | 37.6 | 2 | 220.0 | 40.0 |
| 186 | −905.6 | 156.4 | 55.2 | 184.7 | 27.8 | 14.4 | −47.9 | 2 | 220.0 | 40.0 |
| 188 | −947.1 | 19.1 | −24.7 | 20.6 | 13.0 | 2.5 | 61.7 | 1 | 220.0 | 40.0 |
| 189 | −947.9 | 328.5 | 31.7 | 311.9 | 40.6 | 4.6 | 46.5 | 1 | 209.0 | 24.0 |
| 190 | −976.2 | 222.7 | −3.9 | 224.4 | −27.2 | 6.7 | −46.8 | 2 | 209.0 | 24.0 |
| 191 | −976.4 | 12.0 | 14.1 | 8.2 | 36.9 | 6.9 | 80.1 | 2 | 209.0 | 24.0 |
| 192 | −997.0 | 183.3 | 2.1 | 181.6 | −19.4 | 12.4 | −72.8 | 2 | 209.0 | 24.0 |
| 194 | −1017.8 | 335.0 | 32.7 | 317.8 | 44.0 | 3.5 | 52.4 | 1 | 209.0 | 24.0 |
| 197 | −1055.2 | 9.0 | 39.1 | 333.1 | 55.7 | 13.1 | 65.4 | 2 | 235.0 | 35.0 |
| 198 | −1055.9 | 3.4 | 27.1 | 355.7 | 50.7 | 14.5 | 84.3 | 2 | 201.3 | 25.3 |
| 202 | −1121.1 | 336.6 | 2.3 | 332.9 | 19.9 | 4.1 | 59.4 | 1 | 201.3 | 25.3 |
| 203 | −1121.7 | 351.6 | 36.8 | 334.6 | 57.0 | 10.6 | 66.2 | 2 | 201.3 | 25.3 |
| 204 | −1142.1 | 346.9 | 11.8 | 340.6 | 32.0 | 2.6 | 69.6 | 1 | 201.3 | 25.3 |
| 206 | −1179.9 | 356.4 | 16.5 | 350.1 | 38.9 | 13.4 | 79.7 | 2 | 201.3 | 25.3 |
| 134 | −1184.9 | 348.3 | 21.0 | 328.0 | 56.5 | 8.5 | 61.3 | 1 | 193.0 | 42.0 |
| 133 | −1190.9 | 185.3 | 28.2 | 186.0 | −13.5 | 19.3 | −69.0 | 2 | 193.0 | 42.0 |
| 132 | −1191.9 | 355.5 | −10.2 | 353.1 | 29.8 | 9.9 | 77.2 | 2 | 193.0 | 42.0 |
| 131 | −1196.6 | 334.0 | −56.3 | 351.3 | −19.3 | 6.4 | 52.0 | 2 | 193.0 | 42.0 |
| 113 | −1291.4 | 347.3 | −22.3 | 349.4 | 9.3 | 7.9 | 65.4 | 2 | 198.2 | 36.1 |
| 114 | −1291.8 | 315.6 | −9.4 | 316.0 | 7.8 | 13.0 | 42.1 | 2 | 198.2 | 36.1 |
| 111 | −1312.7 | 165.9 | 8.1 | 163.3 | −22.3 | 9.5 | −68.0 | 1 | 198.2 | 36.1 |

(*continued on next page*)

**Table A2** (*continued*)

| Spl ID | Level (m) | $D_g$ (°) | $I_g$ (°) | $D_s$ (°) | $I_s$ (°) | MAD (°) | VGP (°N) | Q | Dip az. (°N) | Dip (°) |
|---|---|---|---|---|---|---|---|---|---|---|
| 106 | −1356.9 | 337.3 | −18.1 | 342.0 | −1.9 | 5.1 | 57.1 | 1 | 218.2 | 30.4 |
| 104 | −1360.7 | 6.7 | −7.8 | 5.2 | 18.1 | 6.8 | 71.5 | 2 | 218.2 | 30.4 |
| 102 | −1377.2 | 1.1 | −32.1 | 7.2 | −6.7 | 6.4 | 58.8 | 2 | 218.2 | 30.4 |
| 100 | −1380.7 | 347.4 | 7.9 | 339.7 | 25.8 | 14.4 | 66.7 | 1 | 218.2 | 30.4 |
| 97 | −1383.1 | 359.7 | −9.4 | 358.8 | 14.5 | 4.3 | 70.3 | 2 | 218.2 | 30.4 |
| 98 | −1383.7 | 6.4 | −14.6 | 6.8 | 11.5 | 1.0 | 67.8 | 1 | 218.2 | 30.4 |
| 155 | −1411.0 | 327.8 | 8.9 | 319.8 | 25.5 | 2.3 | 50.1 | 1 | 201.0 | 30.0 |
| 156 | −1414.0 | 341.9 | 0.3 | 337.7 | 23.1 | 7.3 | 64.2 | 1 | 201.0 | 30.0 |
| 157 | −1427.9 | 326.6 | 15.3 | 315.3 | 30.6 | 8.9 | 47.4 | 2 | 201.0 | 30.0 |
| 162 | −1440.5 | 344.1 | 8.4 | 336.9 | 31.5 | 1.6 | 66.4 | 1 | 201.0 | 30.0 |
| 161 | −1441.4 | 302.2 | −20.1 | 310.7 | −11.9 | 4.4 | 32.0 | 1 | 201.0 | 30.0 |
| 166 | −1480.5 | 146.8 | 16.7 | 152.9 | 16.7 | 22.7 | −45.8 | 2 | 240.0 | 20.0 |
| 170 | −1489.7 | 198.8 | 30.7 | 204.1 | 15.0 | 17.4 | −48.2 | 2 | 240.0 | 20.0 |
| 171 | −1514.6 | 138.0 | −11.6 | 134.8 | −6.8 | 13.6 | −40.8 | 2 | 240.0 | 20.0 |
| 174 | −1527.0 | 138.9 | −18.7 | 133.2 | −13.8 | 1.8 | −41.3 | 1 | 240.0 | 20.0 |
| 175 | −1531.5 | 179.0 | −14.3 | 172.9 | −23.1 | 3.4 | −73.6 | 1 | 240.0 | 20.0 |
| 177 | −1545.1 | 156.4 | −5.6 | 154.1 | −7.4 | 8.4 | −56.0 | 2 | 240.0 | 20.0 |
| 178 | −1545.5 | 184.2 | −33.1 | 170.2 | −42.4 | 12.7 | −80.8 | 1 | 240.0 | 20.0 |
| 136 | −1662.6 | 352.8 | 28.0 | 329.8 | 30.4 | 2.1 | 60.1 | 1 | 248.0 | 39.3 |
| 139 | −1697.6 | 13.4 | 11.9 | 359.1 | 31.2 | 4.1 | 79.7 | 1 | 248.0 | 39.3 |
| 141 | −1702.4 | 322.7 | 31.0 | 306.8 | 14.8 | 2.3 | 36.0 | 1 | 248.0 | 39.3 |
| 142 | −1707.5 | 329.2 | −9.1 | 326.4 | 18.1 | 2.0 | 53.6 | 1 | 200.0 | 43.0 |
| 147 | −1737.5 | 354.2 | −16.8 | 353.3 | 22.1 | 2.8 | 73.2 | 1 | 200.0 | 43.0 |
| 148 | −1737.9 | 344.8 | −21.8 | 346.5 | 14.2 | 2.9 | 66.4 | 1 | 200.0 | 43.0 |
| 150 | −1749.5 | 153.1 | 6.7 | 148.5 | −22.2 | 15.0 | −56.6 | 2 | 200.0 | 43.0 |
| 152 | −1755.1 | 148.5 | −8.4 | 134.3 | −31.8 | 2.5 | −46.8 | 1 | 200.0 | 43.0 |
| 208 | −1761.1 | 118.4 | 32.4 | 141.8 | 14.8 | 5.1 | −39.4 | 1 | 202.0 | 52.0 |
| 213 | −1956.1 | 112.0 | 35.8 | 141.6 | 21.1 | 13.7 | −36.8 | 2 | 202.0 | 52.0 |
| 212 | −1959.7 | 212.7 | 14.5 | 214.9 | −36.6 | 20.1 | −57.5 | 2 | 202.0 | 52.0 |
| 217 | −2047.4 | 329.8 | 27.5 | 317.2 | 11.2 | 12.2 | 44.0 | 2 | 258.0 | 38.0 |
| 218 | −2069.3 | 167.2 | −37.0 | 142.6 | −27.9 | 6.8 | −53.2 | 2 | 258.0 | 38.0 |
| 223 | −2114.4 | 189.8 | −34.3 | 145.6 | −35.9 | 12.2 | −57.8 | 2 | 256.3 | 56.3 |
| 224 | −2132.4 | 58.9 | 12.3 | 35.6 | 63.4 | 27.3 | 56.5 | 2 | 256.3 | 56.3 |
| 225 | −2144.1 | 5.2 | −53.7 | 40.5 | −16.7 | 16.2 | 37.0 | 2 | 256.3 | 56.3 |
| 226 | −2144.8 | 47.0 | −22.4 | 45.7 | 27.4 | 9.6 | 45.7 | 2 | 256.3 | 56.3 |
| 227 | −2164.4 | 23.0 | 2.4 | 6.6 | 31.3 | 4.6 | 78.1 | 2 | 256.3 | 56.3 |
| 229 | −2189.3 | 180.8 | −27.1 | 149.8 | −26.0 | 2.8 | −58.8 | 1 | 256.3 | 56.3 |
| 234 | −2317.8 | 148.6 | −1.4 | 155.1 | 13.9 | 4.3 | −48.2 | 1 | 256.3 | 56.3 |
| 238 | −2360.1 | 177.8 | 42.4 | 207.9 | 14.6 | 13.8 | −46.2 | 2 | 256.3 | 56.3 |
| *Rejected ChRM directions* | | | | | | | | | | |
| 96 | 0.6 | 198.0 | 77.7 | 202.0 | 3.6 | 14.6 | −54.2 | 3 | 203.1 | 74.1 |
| 95 | 0.0 | 244.7 | 17.1 | 256.1 | −37.4 | 5.6 | −21.2 | 2 | 203.1 | 74.1 |
| 94 | −14.0 | 115.0 | 44.6 | 156.9 | 9.8 | 10.1 | −51.0 | 3 | 203.1 | 74.1 |
| 92 | −23.2 | 228.2 | 41.6 | 224.2 | −28.0 | 6.3 | −47.2 | 3 | 203.1 | 74.1 |
| 89 | −26.6 | 250.0 | −20.9 | 306.9 | −45.4 | 2.3 | 15.7 | 3 | 203.1 | 74.1 |
| 84 | −31.6 | 306.1 | 6.5 | 290.3 | 14.2 | 2.3 | 21.3 | 2 | 203.1 | 74.1 |
| 85 | −31.6 | 292.8 | 2.9 | 290.2 | 0.5 | 1.9 | 18.0 | 1 | 203.1 | 74.1 |
| 80 | −52.2 | 300.5 | −5.3 | 300.2 | 5.6 | 1.3 | 28.0 | 1 | 203.1 | 74.1 |
| 79 | −56.7 | 59.3 | 65.9 | 186.1 | 34.5 | 16.5 | −43.6 | 3 | 203.1 | 74.1 |
| 78 | −58.9 | 266.8 | 5.5 | 279.7 | −23.5 | 4.5 | 2.9 | 3 | 203.1 | 74.1 |
| 77 | −85.8 | 329.4 | 27.2 | 270.7 | 39.2 | 4.0 | 10.5 | 2 | 203.1 | 74.1 |
| 74 | −99.9 | 245.8 | 62.4 | 221.5 | −4.9 | 14.5 | −43.3 | 3 | 203.1 | 74.1 |
| 73 | −100.2 | 245.3 | −24.7 | 312.7 | −49.6 | 8.3 | 16.9 | 2 | 203.1 | 74.1 |
| 72 | −101.2 | 67.7 | 62.1 | 179.7 | 34.2 | 10.6 | −44.2 | 3 | 203.1 | 74.1 |
| 71 | −104.3 | 125.2 | 47.1 | 157.0 | 9.6 | 28.7 | −51.1 | 3 | 198.4 | 62.2 |
| 70 | −104.3 | 333.8 | 19.9 | 289.4 | 48.7 | 4.8 | 28.8 | 2 | 198.4 | 62.2 |
| 69 | −107.3 | 291.6 | −9.9 | 298.7 | −1.8 | 6.4 | 24.9 | 2 | 198.4 | 62.2 |
| 60 | −236.9 | 132.1 | −59.8 | 52.9 | −35.6 | 11.4 | 20.6 | 3 | 198.4 | 62.2 |
| 58 | −241.9 | 296.5 | −57.1 | 343.8 | −18.9 | 10.0 | 50.0 | 3 | 198.4 | 62.2 |
| 57 | −244.9 | 297.9 | −48.7 | 336.1 | −14.7 | 11.8 | 48.4 | 3 | 198.4 | 62.2 |
| 56 | −253.0 | 97.5 | 14.6 | 116.6 | 16.2 | 5.3 | −19.2 | 1 | 198.4 | 62.2 |
| 49 | −265.2 | 315.9 | −33.1 | 330.2 | 5.0 | 24.9 | 52.4 | 3 | 198.4 | 62.2 |
| 48 | −268.2 | 313.7 | −16.0 | 315.0 | 13.6 | 17.8 | 42.8 | 3 | 198.4 | 62.2 |
| 47 | −268.6 | 346.4 | 58.7 | 224.9 | 52.0 | 2.6 | −16.6 | 3 | 198.4 | 62.2 |
| 46 | −270.9 | 171.1 | 4.5 | 154.9 | −48.3 | 12.0 | −67.8 | 3 | 198.4 | 62.2 |
| 44 | −272.0 | 291.6 | −7.0 | 296.1 | −0.5 | 7.6 | 22.9 | 3 | 198.4 | 62.2 |
| 43 | −283.0 | 317.5 | −16.6 | 317.7 | 16.2 | 15.5 | 45.8 | 3 | 198.4 | 62.2 |
| 42 | −290.9 | 315.1 | −36.5 | 332.5 | 2.4 | 7.2 | 53.1 | 3 | 198.4 | 62.2 |
| 37 | −301.0 | 137.4 | −15.9 | 106.7 | −32.7 | 5.6 | −22.5 | 1 | 198.4 | 62.2 |
| 34 | −311.2 | 41.6 | −41.1 | 36.6 | 17.8 | 6.8 | 51.1 | 3 | 198.4 | 62.2 |
| 33 | −312.1 | 247.8 | 3.4 | 263.3 | −33.2 | 9.3 | −13.9 | 3 | 198.4 | 62.2 |
| 32 | −326.2 | 224.1 | 53.1 | 213.6 | −6.1 | 13.9 | −49.9 | 3 | 198.4 | 62.2 |
| 31 | −326.4 | 324.5 | −23.5 | 327.6 | 17.0 | 9.8 | 54.3 | 3 | 198.4 | 62.2 |
| 30 | −329.9 | 358.1 | −50.6 | 5.5 | 9.6 | 6.5 | 67.2 | 3 | 198.4 | 62.2 |

**Table A2** (*continued*)

| Spl ID | Level (m) | $D_g$ (°) | $I_g$ (°) | $D_s$ (°) | $I_s$ (°) | MAD (°) | VGP (°N) | Q | Dip az. (°N) | Dip (°) |
|---|---|---|---|---|---|---|---|---|---|---|
| 27 | −342.1 | 119.8 | 5.0 | 118.2 | −7.7 | 3.7 | −26.8 | 1 | 198.4 | 62.2 |
| 28 | −342.5 | 142.6 | −21.2 | 102.8 | −39.2 | 5.4 | −20.8 | 1 | 198.4 | 62.2 |
| 19 | −383.7 | 141.6 | −15.7 | 108.9 | −36.3 | 5.2 | −25.3 | 1 | 198.4 | 62.2 |
| 18 | −394.9 | 141.3 | −16.4 | 107.9 | −36.4 | 5.1 | −24.5 | 1 | 198.4 | 62.2 |
| 16 | −401.8 | 218.2 | 32.8 | 216.5 | −18.5 | 10.3 | −51.4 | 3 | 203.3 | 52.7 |
| 129 | −673.0 | 336.1 | 39.4 | 282.8 | 64.4 | 8.1 | 27.7 | 3 | 190.0 | 44.0 |
| 127 | −682.7 | 349.4 | 16.1 | 333.4 | 55.5 | 8.5 | 65.7 | 3 | 190.0 | 44.0 |
| 128 | −682.9 | 331.3 | 1.3 | 321.1 | 33.9 | 11.3 | 53.3 | 3 | 190.0 | 44.0 |
| 123 | −712.7 | 3.7 | −4.5 | 1.9 | 39.2 | 6.5 | 84.8 | 3 | 190.0 | 44.0 |
| 124 | −712.9 | 316.5 | 16.5 | 295.5 | 36.9 | 2.2 | 31.3 | 3 | 190.0 | 44.0 |
| 180 | −807.8 | 310.3 | −68.1 | 8.1 | −45.2 | 11.7 | 35.6 | 3 | 220.0 | 40.0 |
| 185 | −884.8 | 191.0 | 35.4 | 196.7 | −0.8 | 12.0 | −58.9 | 3 | 220.0 | 40.0 |
| 193 | −997.7 | 340.8 | 7.7 | 335.6 | 23.0 | 5.4 | 62.6 | 3 | 209.0 | 24.0 |
| 199 | −1056.8 | 209.5 | −6.6 | 210.9 | −31.6 | 19.7 | −59.8 | 3 | 201.3 | 25.3 |
| 201 | −1092.6 | 170.8 | 40.3 | 177.3 | 17.7 | 15.8 | −53.8 | 3 | 201.3 | 25.3 |
| 200 | −1092.9 | 273.7 | 10.3 | 271.1 | 2.0 | 5.8 | 1.4 | 3 | 201.3 | 25.3 |
| 205 | −1142.5 | 106.7 | 37.3 | 125.5 | 35.1 | 11.9 | −19.7 | 3 | 201.3 | 25.3 |
| 130 | −1196.0 | 234.2 | 12.5 | 235.9 | −19.3 | 12.9 | −34.8 | 3 | 193.0 | 42.0 |
| 119 | −1233.7 | 353.1 | −4.9 | 349.7 | 27.5 | 10.2 | 74.3 | 3 | 198.2 | 36.1 |
| 117 | −1250.3 | 348.1 | −6.2 | 344.9 | 24.8 | 11.8 | 70.1 | 3 | 198.2 | 36.1 |
| 115 | −1271.0 | 348.1 | −7.4 | 345.3 | 23.7 | 10.2 | 69.9 | 3 | 198.2 | 36.1 |
| 116 | −1271.8 | 350.0 | 9.3 | 340.7 | 40.0 | 8.6 | 72.0 | 3 | 198.2 | 36.1 |
| 110 | −1315.7 | 148.9 | 18.6 | 151.9 | −6.1 | 29.5 | −54.0 | 3 | 198.2 | 36.1 |
| 108 | −1333.7 | 150.9 | −13.3 | 141.2 | −22.8 | 15.9 | −50.6 | 3 | 218.2 | 30.4 |
| 105 | −1356.2 | 167.0 | −4.4 | 160.9 | −22.5 | 4.4 | −66.4 | 3 | 218.2 | 30.4 |
| 159 | −1439.2 | 6.6 | −0.4 | 4.5 | 28.6 | 6.3 | 77.5 | 3 | 201.0 | 30.0 |
| 160 | −1440.1 | 4.1 | −14.6 | 4.1 | 14.2 | 5.0 | 69.8 | 3 | 201.0 | 30.0 |
| 164 | −1477.1 | 334.1 | −14.1 | 338.7 | −11.9 | 27.4 | 51.0 | 3 | 240.0 | 20.0 |
| 168 | −1479.5 | 341.5 | −47.9 | 360.0 | −40.7 | 15.5 | 39.7 | 3 | 240.0 | 20.0 |
| 172 | −1514.6 | 115.1 | −37.3 | 105.8 | −24.4 | 4.2 | −19.7 | 1 | 240.0 | 20.0 |
| 173 | −1525.9 | 317.6 | 0.0 | 318.3 | −4.2 | 4.3 | 40.4 | 3 | 240.0 | 20.0 |
| 179 | −1546.2 | 334.9 | 41.0 | 317.7 | 39.7 | 8.1 | 51.5 | 3 | 240.0 | 20.0 |
| 137 | −1675.8 | 43.0 | −6.8 | 39.4 | 28.6 | 14.2 | 51.6 | 3 | 248.0 | 39.3 |
| 143 | −1716.3 | 296.4 | −2.1 | 296.1 | 2.8 | 6.5 | 23.8 | 2 | 200.0 | 43.0 |
| 144 | −1721.4 | 185.7 | 47.4 | 190.3 | 5.2 | 25.1 | −58.7 | 3 | 200.0 | 43.0 |
| 146 | −1735.2 | 161.1 | 34.0 | 168.6 | −1.8 | 29.3 | −61.6 | 3 | 200.0 | 43.0 |
| 210 | −1768.1 | 78.5 | 29.0 | 118.6 | 42.7 | 4.7 | −11.3 | 1 | 202.0 | 52.0 |
| 214 | −1977.5 | 99.1 | 43.0 | 143.5 | 33.3 | 12.2 | −32.6 | 3 | 202.0 | 52.0 |
| 216 | −2043.3 | 325.9 | 22.5 | 317.2 | 5.0 | 15.1 | 42.3 | 3 | 258.0 | 38.0 |
| 220 | −2084.0 | 327.5 | −11.2 | 338.7 | −21.4 | 15.2 | 46.6 | 3 | 258.0 | 38.0 |
| 222 | −2084.9 | 1.6 | 4.6 | 351.0 | 15.3 | 10.9 | 68.9 | 3 | 256.3 | 56.3 |
| 231 | −2251.0 | 209.8 | 39.5 | 222.1 | −5.1 | 29.4 | −42.9 | 3 | 256.3 | 56.3 |
| 232 | −2281.1 | 32.6 | 14.2 | 1.8 | 46.0 | 4.9 | 88.4 | 3 | 256.3 | 56.3 |
| 233 | −2308.4 | 20.6 | 69.0 | 280.3 | 43.3 | 7.6 | 19.8 | 2 | 256.3 | 56.3 |
| 236 | −2345.1 | 119.1 | 7.6 | 142.7 | 42.7 | 10.1 | −26.9 | 3 | 256.3 | 56.3 |
| 237 | −2359.1 | 147.6 | −21.8 | 138.0 | 2.4 | 18.9 | −40.7 | 3 | 256.3 | 56.3 |

some significant gaps in the sampling, 19 polarity zones have been identified in the two sections. These results allow for correlations that are constrained by the independent thermochronological data. Ages of transition of LS to MS and MS to US, inferred from these correlations, are similar to those found in the central and western Himalayan Siwalik Group. This similarity implies that, notwithstanding the differences in the position of different stratigraphic sections and the difference in the local depositional environments, major lithologic changes were broadly synchronous across the strike of the foreland basin. Nevertheless, the Kameng section presents some clear differences with respect to Siwalik sections in the central and western foreland, including an upward decrease in sedimentation rate and a greater thickness of the MS. These differences may be related to the presence of the Shillong Plateau to the south and the influence it had on the drainage pattern and the deformation of the Indian plate.

## Acknowledgments

This research was funded by an INSU Relief de la Terre Grant (2007–2009) awarded to P. Huyghe. G. Dupont-Nivet acknowledges support from the Netherlands Organization for Scientific Research (NWO). We acknowledge the thoughtful reviews by Editor Peter Clift and an anonymous reviewer, which helped to improve this manuscript.

## Appendix A

See Tables A1 and A2.

## References

Acharyya, S.K., 1994. The Cenozoic foreland basin and tectonics of the eastern sub-Himalaya: problems and prospects. Himalayan Geology 15, 3–21.

Alam, M., Alam, M.M., Curray, J.R., Chowdhury, A.L.R., Gani, M.R., 2003. An overview of the sedimentary geology of the Bengal basin in relation to the regional tectonic framework and basin-fill history. Sedimentary Geology 155, 179–208.

Angevine, C.L., Heller, P.L., Paolo, C., 1990. Quantitative Sedimentary Basin Modeling. AAPG Continuing Education Series, Tulsa, Okhahoma.

Appel, E., Rösler, W., Corvinus, G., 1991. Magnetostratigraphy of the Miocene-Pleistocene Surai Khola Siwaliks in West Nepal. Geophysical Journal International 105, 191–198.

Behrensmeyer, A.K., Quade, J., Cerling, T.E., Kappelman, J., Khan, I., Copeland, P., Roe, L., Hicks, J., Stubblefield, P., Willis, B.J., Latorre, C., 2007. The structure and rate of late Miocene expansion of C4 plants: evidence from lateral variation in stable isotopes in paleosols of the Siwalik Group, northern Pakistan. Geological Society of America Bulletin 119, 1486–1505.

Bernet, M., van der Beek, P., Pik, R., Huyghe, P., Mugnier, J.-L., Labrin, E., Szulc, A., 2006. Miocene to recent exhumation of the central Himalaya determined from combined detrital zircon fission-track and U/Pb analysis of Siwalik sediments, western Nepal. Basin Research 18, 393–412.

Bhandari, L.L., Fuloria, R.C., Sastri, V.V., 1973. Stratigraphy of Assam valley. American Association of Petroleum Geologists Bulletin 57, 643–654.

Bilham, R., Bendick, R., Wallace, K., 2003. Flexure of the Indian Plate and intraplate earthquakes. Proceedings of the Indian Academy of Sciences (Earth and Planetary Sciences) 112, 315–329.

Biswas, S., Coutand, I., Grujic, D., Hager, C., Stockli, D., Grasemann, B., 2007. Exhumation and uplift of the Shillong Plateau and its influence on the eastern Himalayas: new constraints from apatite and zircon (U–Th–[Sm])/He and apatite fission track analyses. Tectonics 26, TC6013.

Burbank, D.W., Beck, R.A., Mulder, T., 1996. The Himalayan foreland basin. In: Yin, A., Harrison, M. (Eds.), Asian Tectonics. Cambridge University Press, pp. 149–188.

Chirouze, F., 2011. Exhumation et évolution du drainage himalayen depuis 15 Ma: Apport des archives sédimentaires. PhD thesis. Université de Grenoble, 200 p.

Cina, S.E., Yin, A., Grove, M., Dubey, C.S., Shukla, D.P., Lovera, O.M., Kelty, T.K., Gehrels, G.E., Foster, D.A., 2009. Gangdese arc detritus within the eastern Himalayan Neogene foreland basin: Implications for the Neogene evolution of the Yalu-Brahmaputra River system. Earth and Planetary Science Letters 285, 150–162.

Clark, M.K., Bilham, R., 2008. Miocene rise of the Shillong Plateau and the beginning of the end for the Eastern Himalaya. Earth and Planetary Science Letters 269, 337–351.

DeCelles, P.G., Currie, B.S., 1996. Long-term sediment accumulation in the Middle Jurassic-early Eocene cordilleran retroarc foreland basin system. Geology 24, 591–594.

DeCelles, P.G., Giles, K.N., 1996. Foreland basin systems. Basin Research 8, 115–153.

DeCelles, P.G., Gehrels, G.E., Quade, J., Ojha, T.P., Kapp, P.A., Upreti, B.N., 1998. Neogene foreland basin deposits, erosional unroofing, and the kinematic history of the Himalayan fold-thrust belt, western Nepal. Geological Society of America Bulletin 110, 2–21.

DeCelles, P.G., Gehrels, G.E., Quade, J., LaReau, B., Spurlin, M., 2000. Tectonic implications of U–Pb zircon ages of the Himalayan orogenic belt in Nepal. Science 288, 497–499.

Dekkers, M.J., Passier, H.F., Schoonen, M.A.A., 2000. Magnetic properties of hydrothermally synthesized greigite ($Fe_3S_4$)—II. High- and low-temperature characteristics. Geophysical Journal International 141, 809–819. doi:10.1046/j.1365-246x.2000.00129.x.

Dunlop D. and Özdemir Ö. (1997). Rock Magnetism: Fundamentals and Frontiers. Cambridge University Press.

Dupont-Nivet, G., Lippert, P.C., van Hinsbergen, D.J.J., Meijers, M.J.M., Kapp, P., 2010. Paleolatitude and age of the Indo-Asia collision: paleomagnetic constraints. Geophysical Journal International 182, 1189–1198.

Dutta, S.K., 1980. Palynostratigraphy of the sedimentary formations of the Arunachal Pradesh – 2. Palynology of the Siwalik equivalent rocks of Kameng District. Geophytology 10, 5–13.

Gansser, A., 1964. The Geology of the Himalayas. Wiley Interscience, New York.

Garver, J.I., Brandon, M.T., Roden-Tice, M.K., Kamp, P.J.J., 1999. Exhumation history of orogenic highlands determined by detrital fission track thermochronology. In: Ring, U. et al. (Eds.), Exhumation Processes: Normal faulting, Ductile Flow, and Erosion. Geological Society [London] Special Publication 154, 283–304.

Gautam, P., Appel, E., 1994. Magnetic-polarity stratigraphy of Siwalik Group sediments of Tinau Khola section in west central Nepal, revisited. Geophysical Journal International 117, 223–234.

Gautam, P., Fujiwara, Y., 2000. Magnetic polarity stratigraphy of Siwalik Group sediments of Karnali River section in western Nepal. Geophysical Journal International 142, 812–824.

Gautam, P., Rösler, W., 1999. Depositional chronology and fabric of Siwalik Group sediments in central Nepal from magnetostratigraphy and magnetic anisotropy. Journal of Asian Earth Sciences 17, 659–682.

Griffing, D.H., Bridge, J.S., Hotton, C.L., 2000. Coastal–fluvial paleoenvironments and plant ecology of the early Devonian (Emsian), Gaspe Bay, Canada. In: Friend, P.F., Williams, B.P.J. (Eds.), New Perspectives on the Old Red Sandstone. Geological Society [London] Special Publication 180, 61–84.

Guillot, S., Charlet, L., 2007. Bengal Arsenic, an Archive of Himalaya Orogeny and Paleohydrology. Journal of Environmental Science & Health: Part A A42, 12.

Hallam, D.F., Maher, B.A., 1994. A record of reversed polarity carried by the iron sulphide greigite in British early Pleistocene sediments. Earth and Planetary Science Letters 121, 71–80.

Hodges, K.V., 2000. Tectonics of the Himalaya and southern Tibet from two perspectives. Geological Society America Bulletin 112, 324–350.

Horng, C.-S., Laj, C., Lee, T.-Q., Chen, J.-C., 1992. Magnetic characteristics of sedimentary rocks from the Tsengwen-chi and Erhjen-chi sections in southwestern Taiwan. Terrestrial, Atmospheric and Oceanic sciences 3, 519–532.

Horng, C.-S., Torii, M., Shea, K.-S., Kao, S.-J., 1998. Inconsistent magnetic polarities between greigite- and pyrrhotite/magnetite-bearing marine sediments from the Tsailiao-chi section, southwestern Taiwan. Earth and Planetary Science Letters 164, 467–481.

Huyghe, P., Galy, A., Mugnier, J.-L., France-Lanord, C., 2001. Propagation of the thrust system and erosion in the Lesser Himalaya: geochemical and sedimentological evidence. Geology 29, 1007–1010.

Huyghe, P., Mugnier, J.-L., Gajurel, A.P., Delcaillau, B., 2005. Tectonic and climatic control of the changes in the sedimentary record of the Karnali River section (Siwaliks of Western Nepal). The Island Arc 14, 311–327.

Jelinowska, A., Tucholka, P., Guichard, F., Lefevre, I., Badaut-Trauth, D., Chalié, F., Gasse, F., Tribovillard, N., Desprairies, A., 1998. Mineral magnetic study of Late Quaternary South Caspian Sea sediments: palaeoenvironmental implications. Geophysical Journal International 133, 499–509.

Johnson, G.D., Zeitler, P., Naeser, C.W., Johnson, N.M., Summers, D.M., Frost, C.D., Opdyke, N.D., Tahirkheli, R.A.K., 1982a. The occurrence and fission-track ages of late Neogene and Quaternary volcanic sediments, Siwalik group, Northern Pakistan. Palaeogeography, Palaeoclimatology, Palaeoecology 37, 63–93.

Johnson, N.M., Opdyke, N.D., Johnson, G.D., Lindsay, E.H., Tahirkheli, R.A.K., 1982b. Magnetic polarity stratigraphy and ages of Siwalik group rocks of the Potwar plateau, Pakistan. Palaeogeography, Palaeoclimatology, Palaeoecology 37, 17–42.

Johnson, N.M., Stix, J., Tauxe, L., Cerveny, P.F., Tahirkheli, A.K., 1985. Paleomagnetic chronology, fluvial processes, and tectonic implications of the Siwalik deposits near Chinji village, Pakistan. Journal of Geology 93, 27–40.

Joshi, A., Tewari, R., Mehrotra, R.C., Chakraborty, T.P., 2003. Plant remains from the Upper Siwalik sediments of West Kameng District, Arunachal Pradesh. Journal Geological Society of India 61, 319–324.

Karunakaran, C., Rao, R.A., 1976. Status of exploration of hydrocarbon in the Himalayan region – contributions to stratigraphy and structure. Geological Society of India Miscellaneous Publications 41, 1–66.

Kent, W.N., Dasgupta, U., 2004. Structural evolution in response to fold and thrust belt tectonics in northern Assam. A key to hydrocarbon exploration in the Jaipur anticline area. Marine and Petroleum Geology 21, 785–803.

Kumar, G., 1997. Geology of the Arunachal Pradesh. Geological Society of India, Bangalore (Sp. Publ.).

Lourens, L.J., Hilgen, F.J., Laskar, J., Shackleton, N.J., Wilson, D., 2004. The Neogene period. In: Gradstein, F.M., Ogg, J.G., Smith, A.G. (Eds.), A Geologic Time Scale. Cambridge University Press, Cambridge, UK, pp. 409–440.

Maher, B.A., Hallam, D.F., 2005. Magnetic carriers and remanence mechanisms in magnetite-poor sediments of Pleistocene age, southern North Sea margin. Journal of Quaternary Sciences 20, 79–94.

Mary, C., Iaccarino, S., Courtillot, V., Besse, J., Aissaoui, D.M., 1993. Magnetostratigraphy of Pliocene sediments from the Stirone River (Po Valley). Geophysical Journal International 112, 359–380.

McFadden, P.L., McElhinny, M.W., 1988. The combined analysis of remagnetization circles and direct observations in palaeomagnetism. Earth and Planetary Science Letters 87, 161–172.

Mehrotra, R.C., Awasthi, N., Dutta, S.K., 1999. Study of the fossil wood from the upper Tertiary sediments (Siwalik) of Arunachal Pradesh, India and its implication in palaeoecological and phytogeographical interpretations. Review of Palaeobotany and Palynology 107, 223–247.

Mitra, S., Priestley, K., Bhattacharyya, A.K., Gaur, V.K., 2005. Crustal structure and earthquake focal depths beneath northeastern India and southern Tibet. Geophysical Journal International 160, 227–248.

Molnar, P., Lyon Caen, H., 1989. Fault-plane solutions and active tectonics of the Tibetan Plateau and its margins. Geophysical Journal International 99, 123–153.

Mullender, T.A.T., van Velzen, A.J., Dekkers, M.J., 1993. Continuous drift correction and separate identification of ferromagnetic and paramagnetic contribution in thermomagnetic runs. Geophysical Journal International 114, 663–672.

Najman, Y., 2006. The detrital record of orogenesis: a review of approaches and techniques used in the Himalayan sedimentary basins. Earth Sciences Reviews 74, 1–72.

Najman, Y., Carter, A., Oliver, G., Garzanti, E., 2005. Provenance of early foreland basin sediments, Nepal: constraints to the timing and diachroneity of early Himalayan orogenesis. Geology 33, 309–312.

Najman, Y., Bickle, M., BouDagher-Fadel, M., Carter, A., Garzanti, E., Paul, M., Wijbrans, J., Willett, E., Oliver, G., Parrish, R., Akhter, S.H., Allen, R., Ando, S., Chisty, E., Reisberg, L., Vezzoli, G., 2008. The Paleogene record of Himalayan erosion: Bengal Basin, Bangladesh. Earth and Planetary Science Letters 273, 1–14.

Nakayama, K., Ulak, P.D., 1999. Evolution of fluvial style in the Siwalik Group in the foothills of the Nepal Himalaya. Sedimentary Geology 125, 205–224.

Ojha, T.P., Butler, R.F., Quade, J., DeCelles, P.G., Richards, D., Upreti, B.N., 2000. Magnetic polarity stratigraphy of the Neogene Siwalik Group at Khutia Khola, far-western Nepal. Bulletin of the Geological Society of America 112, 424–434.

Ojha, T.P., Butler, R.F., DeCelles, P.G., Quade, J., 2009. Magnetic polarity stratigraphy of the Neogene foreland basin of Nepal. Basin Research 21, 61–90.

Opdyke, N.D., Johnson, N., Johnson, G., Lindsay, E., Tahirkheli, R.A.K., 1982. Paleomagnetism of the Middle Siwalik formations of northern Pakistan and rotation of the Salt Range Decollement. Palaeogeography, Palaeoclimatology, Palaeoecology 37, 1–15.

Paul, J., Bürgmann, R., Gaur, V.K., Bilham, R., Larson, K.M., Ananda, M.B., Jade, S., Mukal, M., Anupama, T.S., Satyal, G., Kumar, D., 2001. The motion and active deformation of India. Geophysical Research Letters 28, 647–650.

Perez-Arlucea, M., Smith, N.D., 1999. Depositional patterns following the 1870's avulsion of the Saskatchewan River (Cumberland Marshes, Saskatchewan). Journal of Sedimentary Research 69, 62–73.

Rao, R.A., 1983. Geology and hydrocarbon potential of a part of Assam–Arakan basin and its adjacent areas. Journal Petroleum Asia 1983 (November), 127–158.

Roberts, A.P., Turner, G.M., 1993. Diagenetic formation of ferrimagnetic iron sulphide minerals in rapidly deposited marine sediments, South Island, New Zealand. Earth and Planetary Science Letters 115, 257–273.

Roberts, A.P., Weaver, R., 2005. Multiple mechanisms of remagnetization involving sedimentary greigite ($Fe_3S_4$). Earth and Planetary Science Letters 231, 263–277.

Rowan, C.J., Roberts, A.P., 2006. Magnetite dissolution, diachronous greigite formation, and secondary magnetizations from pyrite oxidation: unravelling complex magnetizations in Neogene marine sediments from New Zealand. Earth and Planetary Science Letters 241, 119–137.
Sagnotti, L., Roberts, A.P., Weaver, R., Verosub, K.L., Florindo, F., Pike, C.R., Clayton, T., Wilson, G.S., 2005. Apparent magnetic polarity reversals due to remagnetization resulting from late diagenetic growth of greigite from siderite. Geophysical Journal International 160, 89–100.
Sanyal, P., Bhattacharya, S.K., Kumar, R., Ghosh, S.K., Sangode, S.J., 2004. Mio-Pliocene monsoonal record from Himalayan Foreland basin (Indian Siwalik) and its relation to the vegetational change. Palaeogeography, Palaeoclimatology, Palaeoecology 205, 23–41.
Singh, G., 1977. On the discovery of vertebrate fossil from the Upper Tertiary of Subansiri district, Arunachal Pradesh. Indian Minerals 29, 65–67.
Singh, S., Chowdhary, P.K., 1990. An outline of the geological framework of the Arunachal Himalaya. Journal of Himalayan Geology 1, 189–197.
Singh, S., France-Lanord, C., 2002. Tracing the distribution of erosion in the Brahmaputra watershed from isotopic compositions of stream sediments. Earth and Planetary Science Letters 252, 645–662.
Singh, T., Prakash, U., 1980. Leaf impressions from the Siwalik sediments of Arunachal Pradesh. Geophytology 10, 104–107.
Singh, T., Tripathi, S.K.M., 1990. Siwalik sediments of the Arunachal Himalaya: palynology, palaeoecology and palaeogeography. Palaeobotanists 38, 325–332.
Sinha, N.K., Chatterjee, B.P., Satsangi, P.P., 1982. Status of palaeotological researches in the North Eastern States of India. Record Geological Society of India 112 (4).
Stewart, R.J., Hallet, B., Zeitler, P.K., Malloy, M.A., Allen, C.M., Trippett, D., 2008. Brahmaputra sediment flux dominated by highly localized rapid erosion from the easternmost Himalaya. Geology 36, 711–714.
Tandon, S.K., 1976. Siwalik sedimentation in a part of the Kumaun Himalaya, India. Sedimentary Geology 16, 131–154.
Tauxe, L., 1998. Paleomagnetic Principles and Practice. Kluwer Academic Publisher, Dordrecht.
Tauxe, L., Kent, V.D., 1984. Properties of a detrital remanence carried by haematite from study of modern river deposits and laboratory redeposition experiments. Geophysical Journal of the Royal Astronomical Society 76, 543–561.
Tensi, J., Mouthereau, F., Lacombe, O., 2006. Lithospheric bulge in the west Taiwan basin. Basin Research 18, 277–299.
Torsvik, T.H., Müller, R.D., Van Der Voo, R., Steinberger, B., Gaina, C., 2008. Global plate motion frames: toward a unified model. Reviews of Geophysics 46, RG3004. doi:10.1029/2007RG000227.
Tric, E., Laj, C., Jehanno, C., Valet, J.-P., Kissel, C., Mazaud, A., Iaccarino, S., 1991. High-resolution record of the Upper Olduvai transition from Po Valley (Italy) sediments: support for dipolar transition geometry. Physics of the Earth and Planetary Interiors 65, 319–336.
Tye, R.S., Coleman, J.M., 1989. Depositional processes and stratigraphy of fluvially dominated lacustrine deltas: Mississippi Delta Plain. Journal of Sedimentary Petrography 59, 973–996.
Upreti, B.N., 1999. An overview of the stratigraphy and tectonics of the Nepal Himalaya. Journal of Asian Earth Sciences 17, 577–606.
Valdiya, K.S., 1980. Geology of the Kumaon Lesser Himalaya. Wadia Institute of Himalayan Geology.
van der Beek, P., Robert, X., Mugnier, J.-L., Bernet, M., Huyghe, P., Labrin, E., 2006. Late Miocene-Recent denudation of the central Himalaya and recycling in the foreland basin assessed by detrital apatite fission-track thermochronology of Siwalik sediments, Nepal. Basin Research 18, 413–434.
Vasiliev, I., Krijgsman, W., Langereis, C.G., Panaiotu, C.E., Matenco, L., Bertotti, G., 2004. Towards an astrochronological framework for the eastern Paratethys Mio-Pliocene sedimentary sequences of the Focsani basin (Romania). Earth and Planetary Science Letters 227, 231–247.
Vasiliev, I., Krijgsman, W., Stoica, M., Langereis, C.G., 2005. Mio-Pliocene magneto-stratigraphy in the southern Carpathian foredeep and Mediterranean–Paratethys correlations. Terra Nova 17, 376–384.
Vasiliev, I., Franke, C., Meeldijk, J.D., Dekkers, M.J., Langereis, C.G., Krijgsman, W., 2008. Putative greigite magnetofossils from the Pliocene epoch. Nature Geoscience 1, 782–786.
White, N.M., Parrish, R.R., Bickle, M.J., Najman, Y.M.R., Burban, D., Maithani, A., 2001. Metamorphism and exhumation of the NW Himalaya constrained by U–Th–Pb analyses of detrital monazite grains from early foreland basin sediments. Journal of the Geological Society 158, 625–635.
Willis, B., 1993. Evolution of Miocene fluvial systems in the Himalayan foredeep through a two kilometer-thick succession in northern Pakistan. Sedimentary Geology 88, 77–121.
Yin, A., 2006. Cenozoic tectonic evolution of the Himalayan orogen as constrained by along-strike variation of structural geometry, exhumation history, and foreland sedimentation. Earth-Science Reviews 76, 1–131.
Yin, A., Harrison, T.M., 2000. Geologic evolution of the Himalayan-Tibetan orogen. Annual Review of Earth and Planetary Sciences 281, 211–280.
Yin, A., Dubey, C.S., Kelty, T.K., Gehrels, G.E., Chou, C.Y., Grove, M., Lovera, O., 2006. Structural evolution of the Arunachal Himalaya and implications for asymmetric development of the Himalayan origin. Current Science 90, 195–206.
Yin, A., Dubey, C.S., Kelty, T.K., Webb, A.A.G., Harrison, T.M., Chou, C.Y., Célérier, J., 2010. Geologic correlation of the Himalayan orogen and Indian craton: Part 2. Structural geology, geochronology, and tectonic evolution of the Eastern Himalaya. Geological Society of America Bulletin 122, 360–395.
Zhu, B., Kidd, S.F., Rowley, D.B., Currie, B.S., Shafique, N., 2005. Age of initiation of the India–Asia collision in the East-Central Himalayas. Journal of Geology 113, 265–285.